MASTER OF SCIENCE IN ELECTRICAL AND ELECTRONIC ENGINEERING

Development of a Realistic Tissue Mimicking Phantom Using Finite Element Method

By

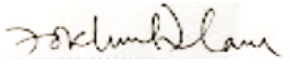**Ahamed- Al- Arifin**

Department of Electrical and Electronic Engineering
Islamic University of Technology (IUT)
Gazipur-1704, Bangladesh.
October, 2021
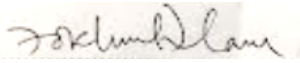
CERTIFICATE OF APPROVAL

The thesis titled "Development of a Realistic Tissue Mimicking Phantom Using Finite Element Method" submitted by Ahamed- Al- Arifin, Student number: 142604 of Academic Year 2014-2015 has been found as satisfactory and accepted as partial fulfillment of the requirement for the degree of Masters of Science in Electrical and Electronic Engineering on 26 October, 2021.
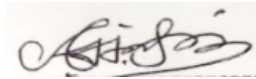
Board of Examiners

1.
……………………………………………..
Prof. Dr. Md. Fokhrul Islam
Professor,
Department of Electrical and Electronic Engineering,
Islamic University of Technology (IUT), Boardbazar, Gazipur.

Chairman
(Supevisor)

2.
……………………………………………..
Prof. Dr. Md. Ruhul Amin
Professor and Head,
Department of Electrical and Electronic Engineering,
Islamic University of Technology (IUT), Boardbazar, Gazipur.

Member
(Ex- Officio)

3.
……………………………………………..
Prof. Dr. Mohammad Rakibul Islam
Professor,
Department of Electrical and Electronic Engineering,
Islamic University of Technology (IUT), Boardbazar, Gazipur.

Member

4.
……………………………………………..
Dr. Md. Taslim Reza
Associate Professor,
Department of Electrical and Electronic Engineering,
Islamic University of Technology (IUT), Boardbazar, Gazipur.

Member

5.
……………………………………………..
Prof. Dr. Muhammad Shahin Uddin
Professor,
Department of ICT,
Mawlana Bhashani Science and Technology University, Tangail

Member
(External)

Declaration of Candidate

It is hereby declared that this Thesis or any part of it has not been submitted elsewhere for the award of any Degree or Diploma.

\---
Prof. Dr. Md. Fokhrul Islam
Supervisor and Professor
Department of Electrical and Electronic Engineering
Islamic University of Technology (IUT)
Gazipur-1704, Bangladesh.

\--------------------------------------
Ahamed- Al- Arifin
Student No.- 142604
Academic Year: 2014-2015

<u>DEDICATION</u>

This thesis is dedicated to my beloved parents and all well-wishers helping me to accomplish this work.

<u>ACKNOWLEDGEMENT</u>

Abstract

In recent medical diagnosis, ultrasound strain imaging or elastography has been established as a useful technique to determine cancerous or abnormal tissues because a malignant tissue is stiffer than benign (normal) tissue. In elastography, the tissue strain is basically estimated from the gradient of tissue displacements and displacements of tissue are estimated from the time delays of gated pre- and post-compression echo signals. Most of the algorithms that are used to find the tissue displacement in elastography are one dimensional that means the displacement is measured only for axial direction which does not provide us with other directional deformation. Moreover, the direct strain imaging techniques are very computational costly that means it took lots of time to compute the data for imaging. To overcome those above discussed problem, this thesis introduces 2-D cross-correlation algorithm to compute time delay which could give us a more realistic reminiscence. In addition to that, the work flow of the strain imaging has been modified to make the imaging less computational costly. Also, to substantiate the above claim MATLAB tic toc function is used to determine each step simulation time of the modified work flow. In this thesis, the presented imaging technique is based on signal correlation. Correlation of signal is typically a measure of similarity of two signals as a function of the displacement of one relative to the other. At first, a 2D finite element tissue mimicking phantom model based on real tissue properties using ANSYS software having a tumor inclusion surrounded by soft tissue is developed. Then, the synthetic tissue was simulated for different inclusion tissue properties for a given displacement. After that, pre- and post-compression data was exported from the ANSYS model. Then, ultrasound simulation (using FIELD II) was done to generate pre- and post-compression RF signal for a more realistic simulation. After that, 2D cross correlation MATLAB function was used to estimate the time delay between pre- and post-compression RF signals. Using MATLAB surf tool, the estimated correlation coefficient was mapped. The map shows a promising result to distinguish between a normal and abnormal tissue. Also, the proposed algorithm offers less computation cost in terms of simulation time with a value of 222.072322 seconds in contrast with the simulation time of the conventional strain imaging having a value more than 222.093015 seconds. So, by applying the above imaging algorithm and procedure to a real world 3-D scenario, we could get a more sophisticated imaging technique which is also computation costly.

Table of Contents

List of Figures

List of Tables

List of Abbreviation & Symbols

Abbreviation & Symbols	Description
RF Signals	Radio Frequency Signals
US	Ultrasound
TDE	Time Delay Estimation
SAD	Sum Absolute Differences
SSD	sum squared differences
X-Corr	Cross-Correlation
1D	One Dimensional
2D	Two Dimensional
3D	Three Dimensional
SONAR	Sound Navigation and Ranging
MATLAB	matrix laboratory
Xcorr2	2D cross-correlation
FEM	Finite Element Method
DOF	Degree of Freedoms
CFD	Computational Fluid Dynamics
CAD	Computer Aided Design
B-Mode	Brightness Mode
ARFI	Acoustic Radiation Force Imaging
ρ	density of the medium or material
c	speed of sound
Z	acoustic impedance of the material
λ	Wavelength of the ultrasound

f	Frequency of the ultrasound
T	Time period of the ultrasound
ϵ	Axial Strain
σ	Stress

CHAPTER 1
INTRODUCTION

1.1 Introduction

Applying mechanical force to understand the behavior of materials is the basis for many aspects of modern engineering practice, from the design of structures to the design of solid propellant rockets [1]. In the early stage of development of mechanics, to study the behavior of materials, loads were often applied to the system until the system failed, then to deduce the characteristics of the material before failure, the failure mechanism was studied. With the advancement of technology, the uses of non-destructive testing procedures were become possible to study the behavior of complex material systems, e.g. X-ray analysis, acoustic behavior and photo-elastic behavior. The results of above testing procedures have played significant role to the development of understanding how materials behave and also to the development of mathematical model that help predict the behavior of more complex material systems [2].

In contrary to the above discussed engineering materials, the biological tissue is not well behaved because they cannot easily be described in close-form mathematical expressions due to the time and moisture dependency. In addition to that, they exhibit different mechanical properties before and after death. Also, these mechanical properties may be age, strain rate and strain range dependent [3]-[6].

Now the elastic properties of biological tissues are usually modified by disease. Surgeons often describe the "feel" of excised abnormal tissues. As a result, a quantitative measure of the elastic properties of tissue should be useful in diagnosing abnormalities. The physical quantities that describe tissue elastic properties are stress, strain, and elastic moduli, and methods have been developed to estimate each of these. Palpation, which has been used for more than 4000 years, utilizes tissue surface stress information to detect tissue abnormalities.

Palpation remains an effective diagnostic tool. In fact, the majority of breast tumors are discovered with palpation. However, palpation is qualitative and lacks sensitivity to small deep abnormalities. Quantitative methods similar to palpation have been developed to visualize

surface pressure. Other recent developments in bio elasticity imaging techniques involve more correctly and non-invasively measuring the tissue strain distribution during external compression. Studies have shown that these techniques show promise in diagnosing and monitoring diseases of the breast, kidney and blood vessels.

The quantitative methods such as non-invasive ultrasound imaging establish as a useful technique as of today for diagnosis of cancerous tissue or benign tumors. To deform the tissue over the region of interest with the help of an ultrasound probe can be performed by applying compression. Because of different stiffness of non-identical tissue gives rise to dissimilar tissue displacement which results different time shifts in the recorded RF signals. The time delay is calculated using the consecutive RF ultrasound echo signals recorded before and after the tissue is compressed. The estimated strain is the axial gradient of the local tissue displacements which are basically calculated from the time delays [7].

1.2 Literature Review

Measuring time-delay estimation of ultrasound echo signal has been a mainstay for a vast range of ultrasound-based signal processing applications. It's a part and parcel of blood flow estimation, tissue elasticity estimation or elastography [8]-[11], tissue velocity estimation [12]-[15] etc. In time-delay estimation, the estimators estimate the displacement between the backscattered signals regarding to the transducer. The measured displacement could be a time-shift or phase-shift between sequences of echo signals [14]. Based on the domain the estimator is operated and the signal the delay estimator could be classified into different classes [16]-[19].

Out of these estimator's time-shift estimator is extensively used in tissue motion estimation. This estimator is basically made of identification of the minimum or maximum of a pattern matching algorithm. The signal in a certain window of the reference signal is fixed to be a pattern and a algorithm is used to match the pattern in the delayed signal. Many patterns matching algorithm is used in these time-delay estimation [16],[20],[21].

Now, the elastography has been a very popular imaging technique for the past two decades. One of the works for elastography is to estimates displacement between pre- and post-compression

RF signal. The estimated displacement is basically a signal as function of time. So, the measured displacement is basically the time delay. Many authors used different algorithms to find out the displacement between pre- and post-compression RF signal.

The most conventional algorithm is the is the time-domain cross-correlation method [8]. The maximum value achieved from the cross-correlation function of the pre- and post-compression RF signals gives us the displacements for the case of time domain cross-correlation method. Other methods such as normalized cross correlation, sum absolute differences (SAD), sum squared differences (SSD) method etc. are used to find time delay [16].

Normalized cross -correlation finds the matching point between signals by looking for the location of highest value in the image matrices [22].

In sum of absolute difference method, a small size region (window) is chosen and it scans an image. For each window of the image, the best matching of the chosen window is searched. A thick map of disparity could be generated by overlapping the chosen window with the window of the searched area [23].

In sum of squared differences window to window measurement is happened. The window subtraction between two images is multiplied, then it is squared. After squaring the summation of squares is calculated. The location of minimum value of the image matrices gives us the matching point [24].

In this research work 2D cross-correlation is used to estimate the displacement between two signals. 2D cross-correlation is the 2D version of the general cross-correlation which is used to find matching of two signals as a function of the displacement of one relative to other [25].

The above-mentioned methods are based the window-based delay estimation technique. In those methods average time shift is calculated for the samples which are contained in the window. The performance of these estimator depends the size of the window and the overlap between windows [26].

The problem regarding the performance of the estimators increases when the time-delay estimator uses multiple window sizes [27],[28]. To improve the performance of the estimator the sample tracking algorithm is better delay estimation algorithm rather than windowing. In this

algorithm, the time shift of each sample of a delayed pulse echo signal is calculated with regards to the reference signal [29].

1.3 Motivation and Methodology

Ultrasound imaging has been a very popular imaging in recent years. The main reason behind this could be the use of a non-invasive technique. To detect the abnormality in human tissue biopsy has been used as medical tool for many years. But doing biopsy of human body is very painful and hazardous because a long and thick needle is use to take the sample from the human body. That means the technique is an invasive technique. So, to overcome this painful a non-invasive ultrasound imaging technique named as elastography was first introduced by J. Ophir in his paper [8]. After introducing, elastography has been developed by many authors in different ways.

In elastography, the imaging of tissue is basically based on the elastic properties of the tissue. Different elastic properties such as strain, stress, Young's modulus etc. are involved in this imaging. The elastography is typically the estimation of strain of a given tissue under a particular stress over the tissue. At first, the ultrasound echoes are gathered before and after the tissue is undergone a small external pressure on the surface by an ultrasound transducer [30]. The acquired ultrasound signal is normally a time-domain signal. Then the strain is estimated using different algorithms from the pre- and post-compression ultrasound echo signals. These algorithms can broadly classify into two groups (1) gradient-based estimation [8], [31]-[35] and (2) direct strain estimation [36]-[39].

The signal acquired from the pre- and post-compression data is basically a time-delay signal. As discussed in the literature review, the algorithm that are used in the time-delay estimation are pattern matching algorithm. The pre- and post- compression signals are divided into windows. In each window there are several echo signals existed. The pre-compression signal played as a reference signal and an algorithm is used to match the pattern in the post-compression signal [16],[20],[21].

Most of the pattern matching algorithm are 1-D algorithm that means they measure the displace for any signal only in axial direction [7],[8],[30],[31]. In this thesis work, a 2-D algorithm named

2-D cross-correlation is used in time-delay estimation which could give us more real scenario of the imaging [40].

Another thing is that the above-mentioned method discussed in literature review, are based on window-based technique. In this technique, average time shift is measured for the samples which are contained in the window. The performance of these windowing estimators declined when it is used multiple window size [27],[28]. To better the performance of these estimators' sample tracking algorithm is used in this thesis work where the delayed echo signal is calculated of each sample regards to the reference signal [29].

Computational cost is one of the major concerns regarding this kind of imaging. So, to reduce the computational cost this thesis work does not deal with strain imaging rather estimate the cross-correlation coefficient using 2-D cross-correlation and map them using MATLAB surf tool [41]. To substantiate that, the proposed method is better than the conventional strain imaging MATLAB tic toc function is used to find the elapsed time for each step for both of the methods we are comparing [7]. The map shows a promising result to distinguish between a normal and abnormal tissue.

1.4 Objectives with specific aims

The main objectives of this research work are to model a tissue mimicking phantom using finite element method and to do the mapping of cross-correlation coefficients using a 2-D time delay estimation technique.

Research objectives are outlined below:
a. To develop a tissue mimicking phantom model using finite element method.
b. To introduce a 2-D time delay estimation technique to find out delays for each delay.
c. To use Young's Modulus as an elastic property of tissue to find the pre- and post-compression data.
d. To reduce the cost of computation of the imaging.
e. To compare the conventional strain imaging with the proposed method.

1.5 Organization of the chapters

Chapter 1 covers the overall introduction of the research with literature review, objectives of the work, motivation and methodology of the research. Chapter 2 covers the history of ultrasound, theory related to ultrasound, working function and different definition related to ultrasound transducer, and tissue mechanics. Chapter 3 discuss about 2-D cross-correlation technique which is used to find the matching between pre- and post-compression RF signal. It also covers description of a finite element method named ANSYS which was used to model the phantom and it also describes the working function of FIELD II program which is a program to simulate the signal in ultrasound environment. Chapter 4 covers the modeling and simulation work of the tissue mimicking phantom model. It also covers the imaging of phantom under ultrasound simulation environment. Chapter 5 discusses the results and discussion regarding the simulation. It also covers the comparison between conventional strain imaging and the proposed method. Chapter 6 discusses about the conclusion and future work related to the research.

CHAPTER 2

ULTRASOUND THEORY

2.1 Introduction to Ultrasound

Ultrasound is used in many different fields. Ultrasonic devices are used to detect objects and measure distances. Ultrasound imaging or sonography is often used in medicine. In the nondestructive testing of products and structures, ultrasound is used to detect invisible flaws. Industrially, ultrasound is used for cleaning, mixing, and accelerating chemical processes. Animals such as bats and porpoises use ultrasound for locating prey and obstacles[42],[43].

2.2 Definition of Ultrasound

Ultrasound is the sound which has the frequency above human hearing (approximately 20kHz). The frequency range corresponds to ultrasound is 100kHz to 50MHz. The characteristics of ultrasound is similar to normal sound wave having sorter wavelength. As it has very short wavelength, it can reflect off a very small surface. This property of ultrasound makes it very helpful for nondestructive testing of materials. Below is given the acoustic spectrum having an ultrasound range divided into further three ranges [42].
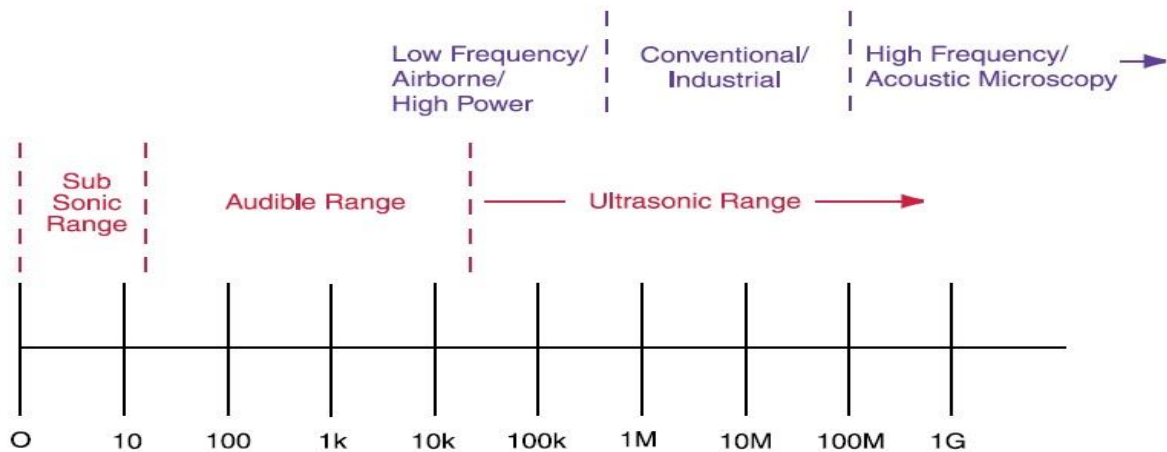
Figure 2.1: The acoustic spectrum [43].

2.3 Historical Events of Ultrasound

The events which are related to the development of the applications of ultrasound in medicine probably starts with the event of measuring distance under water using ultrasound. The process of detecting objects underwater is named as SONAR. So, basically ultrasound scanner can be regarded as kind of 'medical' SONAR [43].

The science of sound called acoustics, probably starts as far back as in the 6th century BC when Pythagoras wrote a book on the mathematical properties of stringed instruments. In 1794, Lazzaro Spallanzani explains Echolocation in bats which is actually the process how the bats hunted and navigate by inaudible sound, not by vision. In 1893, an inventor named Francis Galton invented Galton whistle which produce ultrasound and was used to measure the hearing range of humans and other animals. In 1877, the piezoelectric effect was discovered by the Jacques and Pierre Curie and it was capable to generate and detect the ultrasonic waves in air and water. Then, in 1917 the first use of ultrasound was attempted to detect submarine by Paul Langevin which was a major breakthrough of uses of ultrasound. From then on, the uses of ultrasound have been increases in myriad [44].

2.4 Linear Ultrasound Propagation Theory

Ultrasound is the most commonly used diagnostic imaging modality, accounting for approximately 25% of all imaging examinations performed worldwide nowadays. Ultrasound is an acoustic wave with frequencies greater than the maximum frequency audibles to humans, which is 20 kHz. Diagnostic imaging is generally performed using ultrasound in the frequency range from 2 to 15 MHz. The choice of frequency is dictated by a trade-off between spatial resolution and penetration depth, since higher frequency waves can be focused more tightly but are attenuated more rapidly by tissue. The information in an ultrasonic image is influenced by the physical processes underlying propagation, reflection and attenuation of ultrasound waves in tissue.

Alternating compressions and expansion of a propagation medium produced by a traveling pressure disturbance is called an acoustic wave. This alternating compression and rarefaction are responsible for the displacement of the incremental volumes of the medium and due to the

transfer of the momentum among the incremental volumes, the wave propagates. Each incremental volume does not travel with the pressure disturbance but the medium undergoes some small oscillation about its original position [46].

In real life, the acoustic wave is non-linear in nature and the wave equation of an acoustic wave is very complex to deal with. In this thesis paper, a simple linear wave equation is derived for sound propagation in fluids for simplicity. This linear equation could be a good model for a linear, elastic and isotropic tissue model [46].

Using the Euler's equation and the equation of continuity a pressure plane wave, $p\ (x, t)$, which is propagating through a homogeneous, non-attenuating fluid medium along one spatial dimension, x, can be derived [46].

$$p = \rho c^2 s = \boldsymbol{B}s \text{ (Equation of State for linear acoustic wave)} \tag{2.1}$$

Where, ρ is the medium density, c is the speed of sound, s is the condensation and **B** is the adiabatic bulk modulus.

$$\frac{\partial \rho}{\partial t} + \rho \nabla \cdot u = 0 \quad \text{(Linear equation of continuity)} \tag{2.2}$$

Where ∇ is an operator used in mathematics, u is the velocity of the particle of the medium, and ρ is the density of the medium. The above equation obtrudes that during the propagation of the wave the mass of the medium is constant that means no mass is added or lost. The medium under an external force can be expressed in terms of an equation-

$$\rho \frac{\partial u}{\partial t} + \nabla p = 0 \quad \text{(Linear Eular's equation)} \tag{2.3}$$

From the above three equations the linearized wave equation can be written as:

$$\frac{\partial^2 p}{\partial t^2} = c^2 \nabla^2 p \tag{2.4}$$

An ultrasound image displays the magnitude (absolute value of amplitude) of ultrasound echoes, so a physical understanding of acoustic wave reflection is valuable for interpreting the images.

A reflection is produced when an acoustic wave encounters a difference in acoustic impedance, so an ultrasound image may be thought of as a map of the relative variations in acoustic impedance in the tissues.

If Z is the acoustic impedance for plane wave:

$$Z = \rho c \tag{2.5}$$

2.5 The Acoustic Wave Equation and Simple Solutions

Here, in the first place, a simple linear wave equation for sound propagation is developed. Although, in reality the acoustic wave equation is not linear and much more complicated than this equation presented here. However, this linear approximated equation could be good replica of the real-life one [45].

The acoustic wave is basically a pressure change in a direction. The propagation of an acoustic wave in a direction is mainly caused by the local pressure change which results adjacent fluid to compress which is basically results additional pressure changes [45].

Prior to the derivation of the wave equation, some definitions and explanation related to the wave equation are discussed below-

Production of the wave: A particle displacement (which results further pressure and density change) is made by a transducer (i.e., Piston). The pressure and displacement change affects the immediate region and so on.

Uniform plane wave: The uniform plane wave is a wave where two waves give same magnitude and phase for a given time and they are perpendicular to the direction of propagation.

Particle: In regards to continuum mechanics a particle is something which is consists of a vast number of molecules in it and has a dimension tiny liken to distance for remarkable differences in the acoustic parameters.

Different acoustic parameters can be listed as the pressure experience by the wave, the displacement of the particles within themselves, speed at which the particles are moving, acceleration of those particles, the alternation of the density of the particle, and the potential of the speed or velocity.

Position of the particle, $\vec{r} = x\hat{x} + y\hat{y} + z\hat{z}$ (2.6)

Particle displacement, $\vec{\xi} = \xi_x \hat{x} + \xi_y \hat{y} + \xi_z \hat{z}$ (2.7)

Particle velocity, $\vec{u} = \dfrac{\partial \vec{\xi}}{\partial t}$ (2.8)

Density $= \rho$

Equilibrium density $= \rho_0$

Condensation, $s = \dfrac{\rho - \rho_0}{\rho_0}$ (2.9)

Acoustic pressure, $p = P - P_0$ (2.10)

Where, $P =$ Instantaneous pressures

And $P_0 =$ Pressure when the particles are unperturbed

Three laws used to develop wave equation for fluids [45].

To establish the wave equation for fluids three different laws are used-

1. Equation regarding states-

   The equations regarding states has two criteria's-

   I.   The equation of state is resolved by thermodynamic properties.

   II. The equation of state is different for different material.

2. The continuity equation-

   The continuity equation is based upon the conservation of mass. The changes in density happen due the relative motion of fluid in a volume.

3. Equation of motion-

   The equation of motion is based upon the Newton's 2nd law of motion where the particle motion happens due to the generated force which is caused by change of pressure.

State Equation:

To explain the thermodynamic behavior of the fluid, three physical quantities should be engaged with each other by the equation of state. For instance, the perfect gas's equation of state could be written as follows-

$$P = \rho r T_k \tag{2.11}$$

Here, P is the pressure experienced by the fluid and its unit is in Pascals, ρ is the density of fluid in kg/m³, T_k is the temperature of fluid in Kelvin, and r is the gas constant. For a given gas which has a high thermal conductivity, the gas is isothermic if its compression is slow.

$$\frac{P}{P_0} = \frac{\rho}{\rho_0} \tag{2.12}$$

When the thermal conductivity is low enough, the heat conduction becomes insignificant during a cycle of the acoustic perturbance. In this situation, the condition is represented as an adiabatic condition and for a perfect gas the relation between the pressure and density could be written as follows-

$$\frac{P}{P_0} = \left(\frac{\rho}{\rho_0}\right)^\gamma \tag{2.13}$$

Where, γ is the ratio of specific heats, $\frac{C_p}{C_v}$

The perfect gas is a simple case for an adiabat. To model this relationship, let expand P as a function of ρ (about ρ_0) in a Taylor series:

$$P = P_0 + \left(\frac{\partial P}{\partial \rho}\right)_{\rho_0} (\rho - \rho_0) + \frac{1}{2} \left(\frac{\partial^2 P}{\partial \rho^2}\right)_{\rho_0} (\rho - \rho_0)^2 + \cdots \tag{2.14}$$

The Taylor series shows the fluctuations of P with ρ. We can rewrite this as:

$$P = P_0 + As + \frac{1}{2} Bs^2 + \frac{1}{3} Cs^3 + \cdots \tag{2.15}$$

Where, $$A = \rho_0 \left(\frac{\partial P}{\partial \rho}\right)_{\rho_0} \tag{2.16}$$

$$B = \rho_0{}^2 \left(\frac{\partial^2 P}{\partial \rho^2}\right)_{\rho_0} \qquad (2.17)$$

The Taylor series is nonlinear due to the quadratic term $(\rho - \rho_0)^2$. The nonlinearity of a propagation medium is usually characterized by the ratio of B/A.

We linearize the Taylor series by assuming small fluctuations so that only the lowest order term in $(\rho - \rho_0)$ need be retained. This gives:

$$p = P - P_0 = As \qquad (2.18)$$

Where we define the coefficient A as the adiabatic bulk modulus, **B**:

$$A = \boldsymbol{B} = \rho_0 \left(\frac{\partial P}{\partial \rho}\right)_{\rho_0} \qquad (2.19)$$

Let's examine the unit for $\boldsymbol{B} = \rho_0 \left(\frac{\partial P}{\partial \rho}\right)_{\rho_0}$

P: Pascal where 1 Pa = 1 N/m^2 = 1 kg/s^2/m

ρ: kg/m^3

$$\frac{P}{\rho} \rightarrow \frac{m^2}{s^2}$$

$$\frac{P}{\rho} \rightarrow c^2 \text{ (speed) (experimentally determined)}$$

So,
$$p = \rho_0 c^2 s = \boldsymbol{B}s \qquad (2.20)$$

Is the equation of state for linear acoustic waves in fluids (small changes in density $|s| \ll 1$).

The equation of continuity:

This is essentially a statement of conservation of mass. At first, we are going to investigate at a 1D representation of the fluid particle and then we are going to generalize to 3D representation.
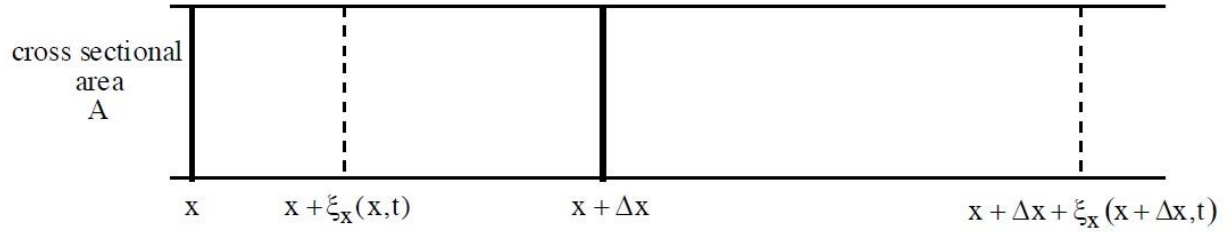
Figure 2.2: 1D representation of a fluid particle [45].

Let's first consider an undisturbed volume of mass $= \rho_0 A \Delta x$.

Then, the mass is disturbed (expands) so that the new volume is:

$$A[x + \Delta x + \xi_x(x + \Delta x, t) - (x + \xi_x(x, t))] = A[\Delta x + \xi_x(x + \Delta x, t) - \xi_x(x, t)] \qquad (2.21)$$

For small Δx

$$\xi_x(x + \Delta x, t) - \xi_x(x, t) \cong \frac{\partial \xi_x}{\partial x} \Delta x \ \text{(approximately)} \qquad (2.22)$$

Giving the new volume

$$A \Delta x \left(1 + \frac{\partial \xi_x}{\partial x}\right) \qquad (2.23)$$

Our disturbed density will then be

$$\rho = \frac{mass}{volume}$$

$$\rho = \frac{\rho_0 A \Delta x}{A \Delta x \left(1 + \frac{\partial \xi_x}{\partial x}\right)} \rightarrow \rho_0 = \rho \left(1 + \frac{\partial \xi_x}{\partial x}\right) \qquad (2.24)$$

Now, recall that the condensation is:

$$s = \frac{\rho - \rho_0}{\rho_0}$$

Solving for the total density gives

$$\rho = s\rho_0 + \rho_0 \qquad (2.25)$$

Substituting into our equation above yields

$$\rho_0 = (s\rho_0 + \rho_0)\left(1 + \frac{\partial \xi_x}{\partial x}\right) \tag{2.26}$$

Or rearranging

$$s\rho_0 = -\rho_0 \frac{\partial \xi_x}{\partial x} - s\rho_0 \frac{\partial \xi_x}{\partial x} \tag{2.27}$$

If we assume that s and $\frac{\partial \xi_x}{\partial x}$ are small so that the second term is negligible (most often the case).

$$s = -\frac{\partial \xi_x}{\partial x} \tag{2.28}$$

Notice that the condensation, s, is the fractional change in density. This equation tells us that if the displacement, ξ_x, varies with x then there is a density change. The minus sign is significant.

If we generalize the equation to 3-D we get

$$s = -\frac{\partial \xi_x}{\partial x} - \frac{\partial \xi_y}{\partial y} - \frac{\partial \xi_z}{\partial z} \tag{2.29}$$

Or

$$s = \left(-\frac{\partial}{\partial x}\hat{x} - \frac{\partial}{\partial y}\hat{y} - \frac{\partial}{\partial z}\hat{z}\right) \cdot \left(\xi_x \hat{x} + \xi_y \hat{y} + \xi_z \hat{z}\right) \tag{2.30}$$

$$s = -\nabla . \vec{\xi} \tag{2.31}$$

If we differentiate with respect to time

$$\frac{\partial}{\partial t}\left(s = -\nabla . \vec{\xi}\right) \tag{2.32}$$

We note that

$$\frac{\partial}{\partial t}\left(-\nabla . \vec{\xi}\right) = -\nabla . \frac{\partial \vec{\xi}}{\partial t} \text{ and } \frac{\partial \vec{\xi}}{\partial t} = \vec{u} \tag{2.33}$$

So, $\qquad \frac{\partial s}{\partial t} = -\nabla . \vec{u} \quad$ (the linear equation of continuity) $\qquad$ (2.34)

Or alternatively if we substitute in for the density we have:

$$\frac{\partial \rho}{\partial t} = -\rho_0 \nabla \cdot \vec{u} \qquad (2.35)$$

The simple force equation: Euler's equation

To derive the equation let's assume a small volume of fluid $(dV = dx\, dy\, dz)$ that is undergone a force in the x-direction. Let's also assume that the fluid element is moving along with the fluid surrounding it and having a mass of dm. At first, the 1D case will be considered and then a generalized 3D case will be derived [45].
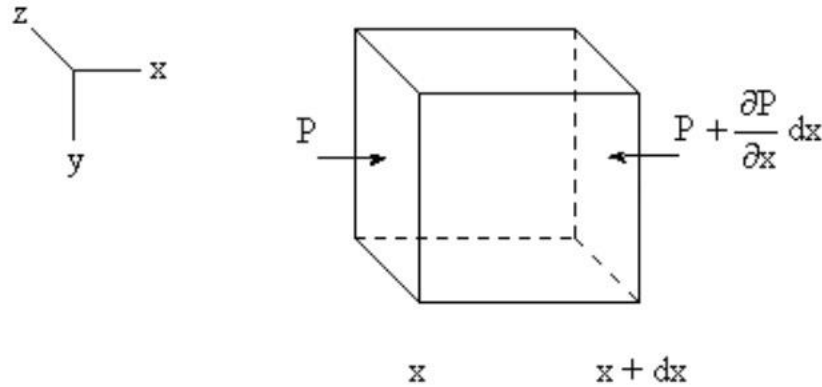
Figure 2.3**:** Small volume of fluid undergoing a force in the x-direction [45].

The force on the fluid from Newton's 2nd law implies:

$$dfm = adm \qquad (2.36)$$

Now the pressure, $P = \frac{force}{area}$, and in the figure we see the force is exerted on the cross-sectional area, $dA = dy\, dz$. Looking at the differential force or pressure across the dm element in the x-direction.

$$df_x = \left[P - \left(P + \frac{\partial P}{\partial x} dx \right) \right] dA \qquad (2.37)$$

16

$$df_x = -\frac{\partial P}{\partial x}dv \tag{2.38}$$

Generalizing to 3 dimensions:

$$\vec{df} = df_x\hat{x} + df_y\hat{y} + df_z\hat{z} \tag{2.39}$$

$$\vec{df} = -\left(\frac{\partial P}{\partial x}\hat{x} + \frac{\partial P}{\partial y}\hat{y} + \frac{\partial P}{\partial z}\hat{z}\right)dv \tag{2.40}$$

$$\vec{df} = -\nabla P dv \tag{2.41}$$

Relating to Newton's 2$^{\text{nd}}$ Law (3D)

$$\vec{df} = \vec{a}dm \tag{2.42}$$

Where,

$$\vec{a} = \frac{d\vec{u}}{dt} \tag{2.43}$$

Recall, there is a difference between

$$\frac{d\vec{u}}{dt} \text{ and } \frac{\partial\vec{u}}{\partial t}.$$

$$\frac{d\vec{u}}{dt} = \frac{\partial\vec{u}}{\partial x}\frac{\partial x}{\partial t} + \frac{\partial\vec{u}}{\partial y}\frac{\partial y}{\partial t} + \frac{\partial\vec{u}}{\partial z}\frac{\partial z}{\partial t} + \frac{\partial\vec{u}}{\partial t} \tag{2.44}$$

Or simplifying

$$\frac{d\vec{u}}{dt} = \frac{\partial\vec{u}}{\partial x}u_x + \frac{\partial\vec{u}}{\partial y}u_y + \frac{\partial\vec{u}}{\partial z}u_z + \frac{\partial\vec{u}}{\partial t} \tag{2.45}$$

$$\vec{a} = \frac{d\vec{u}}{dt} = (\vec{u}.\nabla)\vec{u} + \frac{\partial\vec{u}}{\partial t} \tag{2.46}$$

Using the fact that $dm = \rho dv$ then relating the forces gives

$$-\nabla P dv = \rho\left[(\vec{u}.\nabla)\vec{u} + \frac{\partial\vec{u}}{\partial t}\right]dv$$

$$-\nabla P = \rho\left[(\vec{u}.\nabla)\vec{u} + \frac{\partial\vec{u}}{\partial t}\right] \tag{2.47}$$

This is nonlinear, inviscid force equation (viscosity introduced later as a loss mechanism).

To get the linear Euler's equation we will retain only the 1st order terms.

1st: $p = P - P_0$ $\quad\rightarrow\quad$ $\nabla p = \nabla P$ $\tag{2.48}$

2nd: The particle velocity is assumed small so terms of 2nd order are negligible giving:

$$-\nabla p = \rho\frac{\partial\vec{u}}{\partial t} \tag{2.49}$$

3rd: If we assume that $|s| \ll 1$ (small) then $\rho = \rho_0$ giving finally:

$$-\nabla p = \rho_0\frac{\partial\vec{u}}{\partial t} \quad \text{(linear Euler's equation, Newton's Law)} \tag{2.50}$$

The Linearized wave equation:

Equation of State (Linearized):

$$p = \rho_0 c^2 s = Bs \tag{2.51}$$

Where,

$$B = \rho_0\left(\frac{\partial P}{\partial \rho}\right)_{\rho_0}$$

Continuity equation (Linearized):

$$\frac{\partial \rho}{\partial t} = -\rho_0 \nabla . \vec{u} \tag{2.52}$$

Euler's equation (Linearized):

$$-\nabla p = \rho_0 \frac{\partial \vec{u}}{\partial t} \tag{2.53}$$

To derive the Linear Wave Equation, we first take the derivative of s

Recall,

$$s = \frac{\rho - \rho_0}{\rho_0}$$

So that,
$$\frac{ds}{dt} = \frac{1}{\rho_0}\frac{d\rho}{dt} \qquad \text{or} \qquad \frac{d\rho}{dt} = \rho_0 \frac{ds}{dt}$$

Substituting this into the Continuity equation gives the relative change in density as the divergence of the particle velocity.

$$\rho_0 \frac{\partial s}{\partial t} = -\rho_0 \nabla . \vec{u} \tag{2.54}$$

Substituting in the equation of State yields

$$\frac{\partial}{\partial t}\left[\frac{p}{\boldsymbol{B}}\right] = -\nabla . \vec{u}$$

$$\frac{\partial p}{\partial t} = -\boldsymbol{B}\nabla . \vec{u} \tag{2.55}$$

Taking the derivative of (4) with respect to time gives:

$$\frac{\partial^2 p}{\partial^2 t} = -\boldsymbol{B}\frac{\partial}{\partial t}\nabla . \vec{u} = -\boldsymbol{B}\nabla . \frac{\partial \vec{u}}{\partial t} \tag{2.56}$$

If we take the divergence of Euler's Equation:

$$\nabla.\left[-\nabla p = \rho_0 \frac{\partial \vec{u}}{\partial t}\right]$$

$$-\frac{1}{\rho_0}\nabla^2 p = \nabla.\frac{\partial \vec{u}}{\partial t} \tag{2.57}$$

Substituting into (5) gives the result:

$$\frac{\partial^2 p}{\partial^2 t} = \frac{B}{\rho_0}\nabla^2 p \tag{2.58}$$

Using $\boldsymbol{B} = \rho_0 c^2$ gives us the Linearized Wave Equation:

$$\frac{\partial^2 p}{\partial^2 t} = c^2 \nabla^2 p \tag{2.59}$$

2.6 Definition of Different Ultrasound Parameters

2.6.1 Frequency, Period and Wavelength

Ultrasound vibrations travels in the similar way as the light travels which is in the form of a wave. But one basic difference between these two is that the light travels in a vacuum whereas for ultrasound, it needs an elastic medium such as a solid or liquid. Below is given a shape of a continuous wave having basic parameters of a wave [42]:
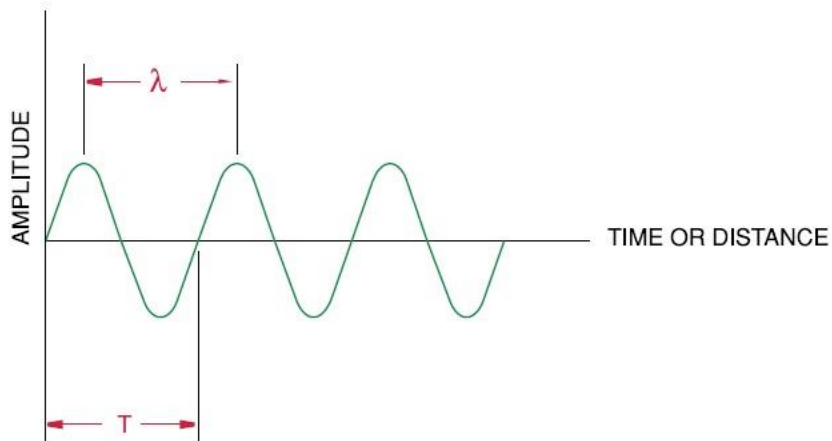
Figure 2 .4: Basic parameters of a continuous wave [42].

The number of cycles completed in one second is called frequency (f) and is measured in Hertz (Hz), some examples follow;

The number of total cycles finished in a second is named as frequency (f) and the unit of the measurement is Hertz (Hz). For instance,

• 1 cycle/second= 1Hz

• 1000 cycles/second= 1kHz

The total time required for completion of one full cycle is called the time period (T), whose unit is in seconds. There is a relation between the frequency and time period which is as follows:

$$f = \frac{1}{T} \tag{2.60}$$

2.6.2 Velocity of Ultrasound and Wavelength

The velocity of ultrasound (c) in a perfectly elastic material at a given temperature and pressure are constant. The relation between c, f, λ and T is given by Equations (2.25) and (2.26):

At a given temperature and pressure, the velocity of ultrasound (c) for a pure elastic material is constant. The relation between c, f, λ and T is given below [42]:

$$\lambda = \frac{c}{f} \tag{2.61}$$

$$\lambda = cT \tag{2.62}$$

$\lambda = $ Wavelength

$c = $ material Sound Velocity

$f = $ Frequency

$T = $ Time period

2.6.3 Wave Propagation and Particle Motion

The most frequently used methods of ultrasound examination use either the longitudinal wave or shear wave. Besides these there are other two sound propagation also exists. One is the surface wave and another one is the lamb wave [42].

- The longitudinal wave is kind of compressional wave where the particle motion is in the direction of propagation of the wave.
- The shear wave is a wave motion where the particle motion is perpendicular to the direction of propagation of the wave.
- Surface wave is a wave motion where the wave has an elliptical particle motion and move across the surface of a material.
- The lamb wave is a wave motion having a complex vibration happening in the material where the thickness f the material is less than the wavelength of ultrasound.
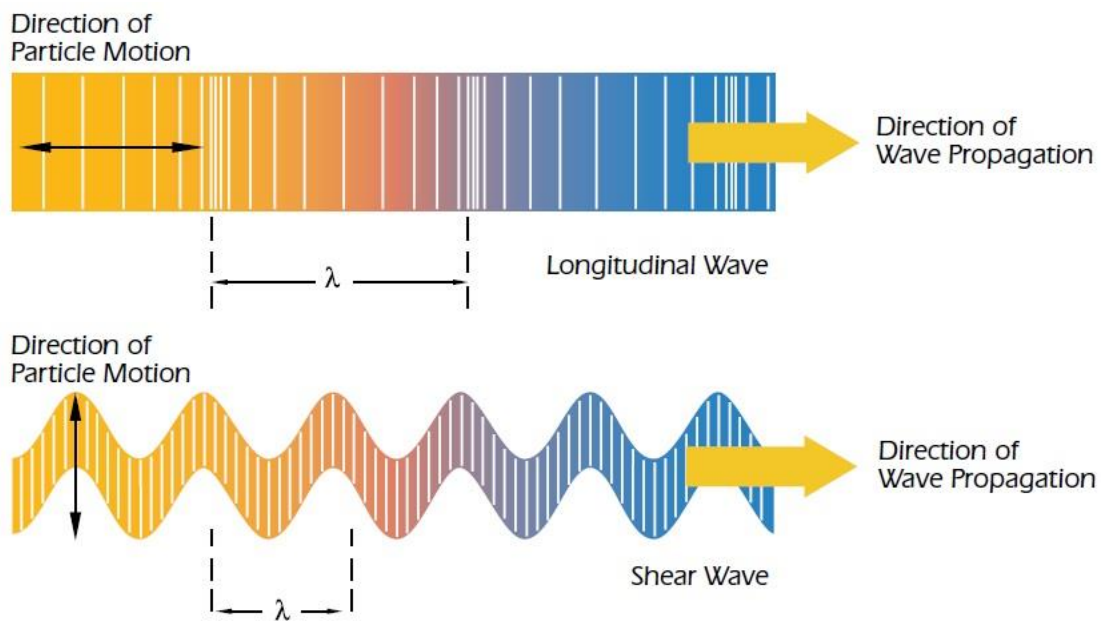
Figure 2.5: An illustration of the particle motion versus the direction of wave propagation for longitudinal waves and shear waves [42].

2.7 Material-Ultrasound Interaction

To acquire information about a test object ultrasonic non-destructive testing provides high frequency sound waves into the test object without altering or damaging the test object. Two primary parameters which are measured in ultrasonic testing are the amount of time for the sound to travel through the sample and another one is the amplitude of the received signal. The thickness of the of material can be calculated using the velocity of sound and round-trip time of flight through the material [42].

$$\boldsymbol{T} = \frac{ct}{2} \tag{2.63}$$

$\boldsymbol{T}$ = Thickness of the Material

c = Velocity of sound through the Material

t = Round trip time of flight

2.8 Sensitivity and Resolution

- Sensitivity of an ultrasound system can be defined as the ability to detect reflectors (or defects) at a given depth foe a test material [42].
- Axial resolution of an ultrasonic system is defined as the capability to generate simultaneous and unique indications from reflectors positioned at nearly the same position with regards to the sound beam [42].
- Near surface of ultrasonic system can be defined as the ability to sense reflectors located near to the surface of the test piece [42].

2.9 Advanced Definition and Formulas Related to Ultrasound

2.9.1 Transducer Waveform and Spectrum

To analyze the frequency of transducer waveform and spectrum the unit of frequency basically considered as MHz, for the analysis of duration of waveform the unit of duration is considered as microseconds, and dB is used for the down to peak amplitude. The following figure explains waveform duration at the -14 dB level or 20% amplitude of peak [42].
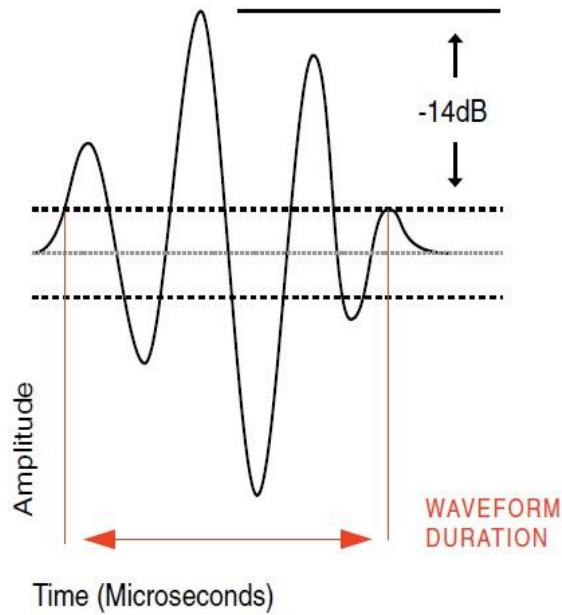
Figure 2.6: Waveform duration at the -14 dB level or 20% amplitude of peak [42].

Figure (5) illustrates peak frequency, upper and lower -6 dB frequencies and MHz bandwidth measurements.
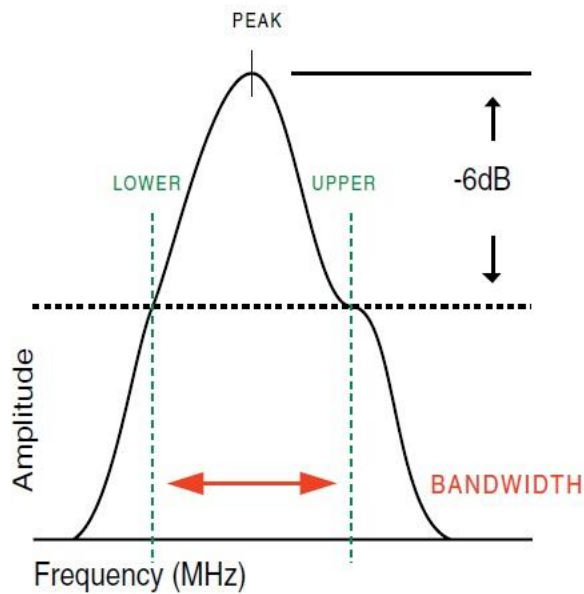
Figure 2.7: The peak frequency, upper and lower -6 dB frequencies and MHz bandwidth measurements [42].

2.9.2 Acoustic Impedance, Reflectivity and Attenuation

The acoustic impedance of a material can be defined as how much resistance an ultrasound beam faces while passing through the material. The equation could be written as follows [42]-

$$Z = \rho c \tag{2.64}$$

Z = Acoustic Impedance

c = Material Sound Velocity

ρ = Material Density

The interface of two different materials having two different acoustic impedance is called as the acoustic interface. When the sound wave hits the acoustic interface some sound energy reflected and some amount get pass through the interface. The sound energy loss in dB during transmission of sound wave from medium 1 to medium 2 is given as follows:

$$dB\ loss = 10\ log_{10} \left[{4Z_1 Z_2}/{(Z_1 + Z_2)^2} \right] \tag{2.65}$$

Z_1 = Acoustic impedance of first impedance

Z_2 = Acoustic impedance of first impedance

The sound energy loss in dB of echo signal in medium 1 reflecting from an interface boundary with medium 2 is given by:

$$dB\ loss = 10\ log_{10} \left[{(Z_2 - Z_1)^2}/{(Z_1 + Z_2)^2} \right] \tag{2.66}$$

2.9.3 Sound Field

The transducer sound field can be divided into two zone: the near field and far field zone. The near field can be defined as zone which is in front of the transducer where the amplitude of sound wave goes through a series of maxima and minima and ends at the last maximum [42].
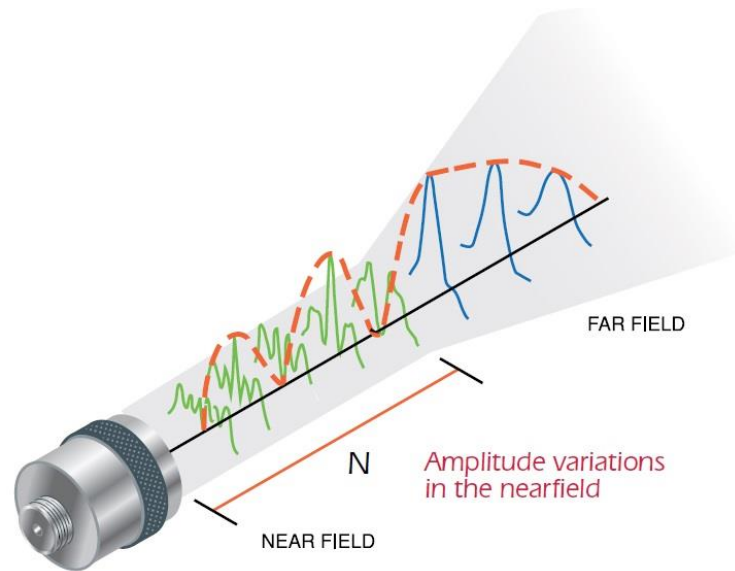
Figure 2.8: The near field and the far field zone of a transducer [42].

As discussed above, the location of the last maximum is near field distance (N) which is the natural focus of the transducer. The field region is beyond the near field region and in this field the wave gradually falls to zero. Due to the variations in amplitude of maxima and minima within the near field, it is very difficult to use the amplitude-based techniques to evaluate the errors precisely. The equation of he near field is given as follows:

$$N = D^2 f / 4c \qquad\qquad (2.67)$$

$$N = D^2 / 4\lambda \qquad\qquad (2.68)$$

$N = $ Near field Distance

$D = $ Diameter of the Element

$f = $ Frequency

$c = $ Velocity of sound through material

$\lambda = $ Wavelength

2.9.4 Focal Zone

The focal zone is basically the narrowest part of the ultrasonic beam in the material and in this we have best spatial resolution. The starting and ending points of this zone is placed where the on-axis pulse-echo signal amplitude drops to -6dB from peak of the focal point. The equation of the focal zone can be written as follows [42]:

$$F_Z = N * S_F^2 \left[2/(1 + .5S_F)\right] \tag{2.69}$$

F_Z = Focal Zone

N = Near Field Distance

S_F = Focal length after normalization

2.10 Ultrasonic Transducer

2.10.1 Definition of Ultrasonic Transducer

Transducer could be defined as any device which converts energy from one form to another form. An ultrasonic transducer is any device which converts electrical energy into mechanical energy in the form of sound wave and vice versa. The ultrasonic transducer consists of mainly the active element, backing and wear plate [42].
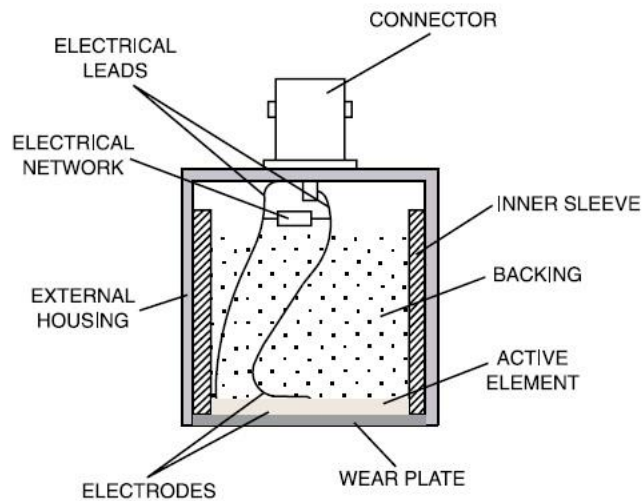
Figure 2.9: An ultrasound transducer [42].

2.10.2 The Active Element

The active element is basically the piezo ferroelectric material. These material converts the electrical energy into mechanical energy and vice versa. In the case of ultrasound simulation, it converts the excitation pulse from a flaw detector into ultrasonic energy. To make these materials the most frequently used material is the polarized ceramics which can be cut in different ways to make different wave modes. Piezo polymers and composites are also used for materials [42].

2.10.3 Backing

The backing is normally used to control the transducer vibration by absorbing the energy which radiated from the back of the active element. The backing in made as a highly attenuative and high dense. The matching acoustic impedance of the backing and active element gives us a heavily damped transducer which shows good range resolution but the signal amplitude may be lower. The mismatch acoustic impedance gives us a transducer which is lower in resolution because of longer waveform duration while it has higher signal amplitude greater in sensitivity [42].

2.10.4 Wear Plate

The main purpose of the transducer ware plate is to safeguard the transducer element from the testing environment. For contact transducers, the material of the wear plate should be sturdy and corrosion resistant in order to withstand the heavy use such as steel. The thickness of the wear surface is selected upon the idea of superposition which permits waves generated by the active element to be in phase with the wave reverberating in the matching layer [42].
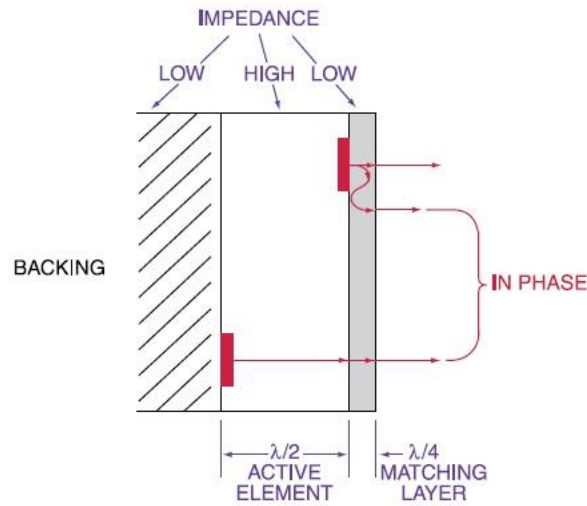
Figure 2.10: The active element and the wear plate when they are in phase [42].

2.10.5 Transducer Excitation

As a general rule, all of our ultrasonic transducers are designed for negative spike excitation. The maximum spike excitation voltages should be limited to approximately 50 volts per mil of piezoelectric transducer thickness. Low frequency elements are thick, and high frequency. Basically, the ultrasonic transducers are made for negative spike excitation as per normal rule. For a piezoelectric transducer thickness the maximum spike excitation voltage should be limited to 50 volts/mil. For low frequency transducer the element is thick while for a high frequency it is thin. For a 5 MHz or lower frequency transducer the used spike excitation signal may be a negative-going 600-volt fast rise time and short duration. The required voltage is halved for a 10 MHz transducer. Instead of negative spike excitation, we can also use the continuous wave or tone burst excitation. The average power dissipation of the transducer should be limited to 125 mW to overcome the overheating [42].

$$V_{rms} = 1/2(0.707)\, V_{p-p} \tag{2.70}$$

$$P_{tot} = \frac{(Duty\ Cycle)(V_{rms})^2 \cos(phase\ angle)}{Z} \tag{2.71}$$

$$No. of\ Cycles\ in\ a\ burst = \frac{(Freq.)(Duty\ Cycle)}{Rep\ Rate} \qquad (2.72)$$

2.11 Introduction to Displacement and Strain

The soft tissue is deformed under the application of a small external force and the governance of this deformation is performed by the mechanical stiffness distribution of the tissue and the force field applied externally. The different tissue mechanics are assumed to be linear, elastic and isotropic materials for the interpretation of the small strain due to the applied small stress [47], [48]. By using the Hook's law, the relationship between this minutely small stress (σ) and strain tensors (ϵ) can be expressed.

$$\sigma_{ij} = c_{ijkl}\epsilon_{kl} \qquad (2.73)$$

Where, c_{ijkl} represents the rank of stiffness constants with the indices i, j, k and l.

The term strain gives us the notion about the amount of deformation for a given displacement locally from a firm body displacement. The Lagrangian finite strain tensor which also named as Green-Lagrangian strain tensor or Green-St-Venant strain tensor is one of the examples of the above such strain for large deformation. This strain could be written as-

$$\epsilon = \frac{1}{2}(C - I) \qquad (2.74)$$

$$C = F^T F \qquad (2.75)$$

Where, C is the Green's deformation tensor and F is the deformation gradient tensor and I is called the Identity matrix.

For small strain the Green-Lagrange strain tensor can be approximated to a linear equation and can be written as follows:

$$\epsilon_{kl} = \frac{1}{2}\left(\frac{\partial u_k}{\partial x_l} + \frac{\partial u_l}{\partial x_k}\right) \qquad (2.76)$$

Where, u_k and u_l are the displacement component is the kth and l^{th} directions respectively and x_k and x_l are the spatial axes. Under applied force, the soft tissue shows more strain than hard tissues. So, strain can be estimated through tissue compression. Considering a constant speed of sound in the tissue, the axial strain could be estimated as follows:

$$\epsilon = \frac{d_2 - d_1}{\Delta y} \qquad\qquad (2.77)$$

Where, Δy is the spatial interval, d_1 is the displacement estimate at distance y and d_2 is the displacement estimate at distance $y + \Delta y$.

CHAPTER 3
THEORIES RELATED TO SIMULATION

3.1 Correlation

In signal processing, correlation is an operation which is used to measure the degree of similarity between two signals to extract information that depends to a large extent on the application. This quantitative measurement of similarity between two signals is basically same as that of a statistical correlation of two random variables, except it is not quantified explicitly by statistical measures like the covariance and standard deviation. We can also define correlation as a direct comparison between the signals based on their actual values at different time instants. Basically, this direct comparison may be quantitatively based upon the amount of the component of one signal contained in the other signal. When it is required to compare two signals quantitively, e.g. *x(n)* and *y(n)*, then a correlation sequence is generated from correlation application which indicates the similarity of the two signals at different time instants. When the two different signals are correlated, then the obtained correlation sequence is known as cross correlation [49].

3.1.1 Cross-Correlation

Now, the cross correlation is widely recognized and used approach to determine the displacements between two images. So, it can also be used to find feature point displacement between deformed and undeformed images. A one-dimensional cross-correlation between two signals $(x(n) and y(n))$ could be defined as follows-

$$r_{xy} = \sum_{n=-\infty}^{\infty} x(n)y(n-l) \qquad\qquad l = 0, \pm 1, \pm 2 \dots. \qquad\qquad (3.1)$$

Or, equivalently, as

$$r_{xy} = \sum_{n=-\infty}^{\infty} x(n)y(n-l) \qquad\qquad l = 0, \pm 1, \pm 2 \ldots. \qquad\qquad (3.2)$$

Where, the index l is the shift or lag parameter.

The cross-correlation between two signals in MATLAB is estimated using the xcorr command. The xcorr (x,y) returns the cross-correlation of two discrete-time sequences. Cross-correlation measures the similarity between a vector x and shifted (lagged) copies of a vector y as a function of the lag. If x and y have different lengths, the function appends zeros to the end of the shorter vector so it has the same length as the other [50].

3.1.2 2-D Cross-Correlation

The cross-correlation between two signals can also be estimated by using the xcorr2 command in MATLAB. The xcorr2(X, Y) returns the cross-correlation of matrices X and Y with no scaling. The xcorr2 command is just the two-dimensional version of the MATLAB command xcorr. The 2-D cross-correlation of an M-by-N matrix, X, and a P-by-Q matrix, H, is a matrix, C, of size M+P-1 by N+Q-1 [40]. Its elements are given by-

$$C(k,l) = \sum_{m=0}^{M-1}\sum_{n=0}^{N-1} X(m,n)\bar{H}(m-k, n-l), \qquad \begin{array}{l} -(P-1) \le k \le M-1 \\[6pt] -(Q-1) \le l \le N-1 \end{array}$$

$$(3.3)$$

Where, the bar over H denotes complex conjugate.

3.2 Finite Element Method or Finite Element Analysis

3.2.1 Introduction to Finite Element Method

The finite element method is a kind of mathematical technique which is basically used to set up and solve a partial differential or an integral equation. To solve an engineering problem by using finite element method what is done is that the system (whose behavior cannot be predicted using closed form equations) is divided into small pieces, or elements whose solution can be approximated.

In finite element method the geometry of the system is defined by a number of points in space which is called nodes. Each node has a certain number of sets of degree of freedoms that may be different for different inputs to the system. Each node is connected with another by elements. The element of a FEM defines as a mathematical interaction of the degree of freedoms (DOFs). For some elements the closed form solution is known e.g., beams and for some elements this solution is unknown e.g., continuum elements. To estimate the unknown solution numerical integration over the element method is used. The above estimation is done by first of all making equation for each element and then combines these equations to form a set of equations which could represent the system to be examined. At last, the set of equations are solved to gain useful information about the characteristics of the system.

One example of these estimation could be given as similarities between a circle and a polygon having infinite number of sides. The polygon having an infinite number of sides could as close as a circle. As it is impossible to make a polygon having infinite number of sides what the FEM does that it's gives us the exact solution to an approximation of the problem. The more the number of elements is used the more the solution is near actual solution. As the number element increases the number equations also increases, so, the simulation gets more computational costly. So, the FEM computer program allows its customer to customize different tools [51].

3.2.2 Uses of Finite Element Method

In terms of manpower and computer resources, the cost required to set up and build a simple finite element model such as cantilever beam is very high compared to its advantages. So, for a

simple model like the above one we had to think about cost-benefits criteria, then, what about the models which are more complex and most real-life models are complicated. Therefore, we need a method which is more sophisticated to handle these compounded situations which leads us to finite element method (FEM) [53].

3.2.3 Basic Procedure for Finite Element Analysis

There are many finite element method software packages available in the market e.g., ANSYS, COMSOL Multiphysics, Nastran etc. Most of them have similar workflow to solve for a finite element problem. Each software package has some procedures to solve the problem. For example, in ANSYS, basically, there are more or less 10 steps to follow for a finite element analysis. These steps are can be sub grouped into three steps. The first sub-group is called the pre-processor, the second might be called as solution step and the third one is called the post-processor. In pre-processor, at first, the model of the geometry is defined, then, the element type is selected. After that, the material properties are assigned to geometry and at last the geometry went into the desired meshing procedure. For the solution procedure, first of all, desired boundary condition is set up along the loads. Then, the model goes under different solution options and last but not the least it is solved under the considering the above conditions. In post-processor, the solved results can be plotted, viewed and we can also export the data. Last of all, we can analyze and checked the output results with the desired results [51].

Pre-processor steps:

1. Define the Solid Model Geometry
2. Select the Element Types
3. Define the Material Properties
4. Mesh

Solution of the geometry steps:

5. Define the Boundary Conditions
6. Define the Loads
7. Set the Solution Options
8. Solve

Post-processor steps:

9. Plot, View, and Export the Results
10. Compare and Verify the Results

3.2.4 A Brief History of ANSYS and Finite Element Analysis

In the beginning of 1940s, the finite element method was first proposed for solving partial differential equations as a numerical analysis. At that time and age, we could do apply the meshing technique and the required set of equations could be find out by the interactions of the elements to solve the equations for the system. The main limitation of that method was still the system of equations had to solve by hand. This problem drew attention to the academics and they were desperate to find a solution. But the success didn't come until the invention of computer with its ability to solve huge system of equations simultaneously. So, due the above reason, the computerized finite element method was ubiquitous among the scientists and engineers.

Although the advent of computerized FEM appeases the laborious handed solution but it was not well enough to solve for every system. It was basically could solve a specific type of problem such as system containing only one type of physics (structural, thermal, etc.) and a single element type (e.g., beams, axisymmetric shells, or plane stress solids). The system was able to solve for multi-element and Multiphysics system [51].

3.2.5 The Development of ANSYS

When NASA was concentrated on researching to have a successful moon landing, the Westinghouse Electric Corporation was trying to build and develop nuclear reactors for space propulsion and nonconventional energy production. The thermal and pressure loads given to the reactor systems were needed to investigate and predict the transient stresses and displacements by the mechanical and nuclear engineers of the Westinghouse Electric Corporation. The above two calculations were both considered as a time and money consuming. So, at that time, an employee of Westinghouse Astro-nuclear Labs in Pittsburg named Dr. John Swanson gave a hypothesis that an integrated, general-purpose finite element program would be time and money efficient for these calculations. Then he himself began to develop a finite element program named STASYS in 1969 for Westinghouse Electric Corporation.

In 1970, Dr. John Swanson left Westinghouse Electric Corporation and established his own company named Swanson Analysis Systems, Inc. (SASI) and there the continued to research and develop his ideas to build a finite element program and named it as ANSYSs. In the first version of ANSYS the program had 40 different types of elements (dampers, springs, beams etc.). In addition to that, there were few elements with thermal degrees of freedom. At the end of that year, Westinghouse Electric Corporation was the first customer buying the program. Soon, the program had become hugely popular and different power industry companies enthusiastically accepted it and use it as if it were a default finite element program. In recent years, ANSYS is one of the paragons of finite element program which ubiquitously used in the area of electrical, mechanical, chemical, civil, aerospace etc. engineering [51].

3.2.6 The Evolution of ANSYS

When the first finite element program was developed in 1970, from then on to today new features and functionality has been added to ANSYS. For instances, in 1975 the first thermoelectric and in1983 the first electromagnetic DOFs of the elements were introduced by ANSYS. The feature of ANSYS were also enriched by interfacing ANSYS with some other products. For instance, the computational fluid dynamics (CFD) capabilities were first

introducing with ANSYS in 1989 by interfacing the SASI's ANSYS and Compuflo's FLOTRAN. Similarly, in 1996 explicit dynamic capabilities ware added to ANSYS by interfacing program from ANSYS and Livermore Software Technology Corporation's LS-DYNAt. Also, in 1992 and in 1994 SASI bought Compuflo and FOTRAN respectively and incorporate the feature of these program into ANSYS.

SASI was purchased by TA associates and named it as ANSYS, Inc in 1994. In the late 1990s, ANSYS emerged themself not only as a single program software but also as a portfolio of simulation products by owning ICEM CFD in 2000, CFX in 2003, and fluent in 2006 which strengthen their computational fluid dynamics offerings. To strengthen their explicit dynamics capabilities ANSYS owned Century Dynamics in 2005 to add AUTODYNs. The ANSYS Inc. continued to developed new products and technologies. For example, in 2009 it released its revised version (revision 12.0) where it introduced us with new explicit dynamics product named ANSYS Explicit STRt. In 1990s, a new user-friendly platform was introduced named ANSYS Workbench. It was introduced to make a bridge between the then existing ANSYS Inc. technology with new feature like improved solid modeling and more stable CAD importation [51].

3.2.7 Today's ANSYS

In recent versions of ANSYS Inc., the program provides with a wide variety of applications including general purpose and specific purpose uses. The specific purpose applications include electronics, turbo machinery, and offshore structures etc. some applications needed a few steps while other applications needed all FEM steps for the simulation [51].

3.3 FIELD II: Ultrasound Simulation Software

3.3.1 Introduction to FIELD II

Field II is an ultrasound program which is used to simulate ultrasound transducer and to do ultrasound imaging for linear acoustics. Field II offers a simulation which is linear and it does not take in consideration the reverberations, multiple scattering etc. Although it has the above

limitations, it can be concluded that it is reliable, powerful, and pragmatic program for the ultrasound simulation. To calculate the pulse ultrasound fields the field program utilize the Tupholme-Stepanishen technique based on spatial impulse response method. For both the pulse wave and continuous wave for many transducers, the program can be simulated. Besides calculating the emitted field, the program can also calculate the pulse echo field. The program can simulate any kind of linear imaging along with the imaging of realistic human tissue. The program can be run on different operating system platform such as Windows, Mac OS, Linux under the MATLAB platform [52],[54].

3.3.2 The spatial impulse response

The field program is based on the concept of spatial impulse response described in a series of paper [9,10,11] which is developed by Tupholme and Stepanishen. The program could be simulated for both the pulse and continuous wave case to find the ultrasound field relying on linear system theory. This simulation is done through the spatial impulse response. The spatial impulse response provides the emitted ultrasound field for a given point as function of time while the transducer is excited by dirac delta function. The convolution of the spatial impulse response and the excitation signal gives us the field for any kind of excitation. As the impulse response is varied as function of position relative to the transducer that is why it is named as spatial impulse response [52].

3.3.3 Simulation of FIELD II

The spatial impulse response is calculated by many authors for different transducer geometries. It is very difficult to calculate a solution while the apodization is take into account. In this case, the transducer surface does not vibrate as a piston. The field program avoids this problem by slicing the transducer surface into squares and the total response is the sum of response of these squares. Hence, the simulation can be done for any transducer geometry and any apodization.

The time required for one simulation is vital concern. To make the simulation simple, it is feasible to use the far field approximation as the squares makes the transducer small. Lowering of sampling frequency might be another solution to down the simulation time [52].

3.3.4 Uses of FIELD II

To start the field program at first the field_init command is executed. By calling the field_init program with an argument of 0, suppresses the splash graphic, and argument -1 suppresses all the notices that the field is started with. After starting of the program, the commands of the field program can be terminated by executing field_end command or by quitting the matlab. Matlab addpath command is used for the directory containing field to include in matlab's search path. Below an example is given for the above execution [53]:

Example: Add the Field directory to the path and start field:
>> addpath('my/copy/of/field/is/here')
>> field_init;

The field program starts with some default values for the simulation. These values consist of the sampling frequency of 100 MHz for all signals involved in the simulation, the speed of sound which is assumed to 1540 m/s and the attenuation of the medium is assumed to 0dB/cm/MHz. These default values can be changed by the user using the set_field command. All the measurements are set using the MKS unit, that means all the distances are in meters, times are seconds and the frequencies are in Hz. The z-axis of the coordinate arrangement represents the aial direction (away from the transducer), the x-axis represents the lateral direction (left to right across an array), and the y-axis represents the elevational direction (out of the scan plane). Most of simulations in the field program follows a standard plan. A conventional measurement of the acoustic field can be parted into the following steps [53]:

- Describe transducer type and make transducer/handle.
- Describe electromechanical impulse response.
- Describe excitation signal.
- Calculate field at each point of interest.

A conventional imaging simulation is similar:

- Describe transducer type and create transducer /handle.

- Describe electromechanical impulse response.

- Describe excitation signal.

- Place initial scatterer and beam positions

- Calculate the echo signal

- Carry the beam and/or scatterers to next position and repeat

Command	Description
xdc_piston	Flat (unfocused) circular piston
xdc_concave	Concave (focused) circular piston
xdc_linear_array	1D linear (phased) array, no elevation focusing
xdc_focused_array	1D linear (phased) array with fixed elevation focus
xdc_focused_multirow	1.75D linear (phased) array with fixed and electronic elevation focus
xdc_2d	2D array

Table 3.1: Transducer making commands.

3.3.5 Transducer type

The field program consists of a number of commands for making a transducer. A small list of the transducers is listed on the above table. Each of the transducer types commands hold a set of parameters and the command gives back handle to the transducer. These transducers are made with their center at (0,0,0) directed towards the +z direction and it cannot be moved. A example of a transducer type is given below [53]:

Example: To make an unfocused circular transducer with a radius of 5mm divided into 0.4mm simulation elements, we use the xdc_piston command.

>> piston = xdc_piston (0.005,0.0004);

piston is now the handle for this transducer; we will use it to work with this transducer.

3.3.6 Electromechanical Impulse Response

It is also called the impulse response. It is the signal which defines by velocity of the transducer face in replies to the application of an electrical impulse. This impulse response actually defines the range of frequencies to which the transducers are sensitive to. Basically, the generated default impulse response is an impulse. To get a manipulated impulse response, one should use the xdc_impulse command. This xdc_command returns nothing as output while taking transducer handle and a vector of samples of the impulse response as its input. The default sample rate of the field program is 100MHz. Following is an example of the field program for impulse response [53]:

Example: To place the impulse response for a transducer which is a circular piston to become a gaussian-enveloped sinusoid centered at 3 MHz with a -8dB bandwidth of 60%.

The Matlab's gauspuls command in the signal processing toolbox to make the samples of the impulse response.

>> fs=100e6; BWR=0.6;

>> tc=gauspuls('cutoff',3e6, BWR,-8,-40);

>> imp_resp=gauspuls(-tc:1/fs:tc,3e6, BWR);

>> xdc_impulse(piston,imp_resp);

3.3.7 Excitation Signal

The xdc_excitation command is used to set the driving voltage applied to the transducer. This command takes transducer handle and a vector of samples of the impulse response as its input

which is similar to xdc_impulse command. The samples here is basically the voltage applied to the transducer which is use to generate an ultrasound signal [53].

Example: To model a circular piston driven by a 15 cycle long, 3MHz tone burst.

```
>> Ncyc=15; fs=100e6; f0=3e6;
>> t_ex=0:1/fs:Ncyc/f0;
>> ex_pulse=sin(2*pi*f0*t_ex);
>> xdc_excitation(piston,ex_pulse);
```

3.3.8 Field calculation

By defining the transducer geometry, impulse response, and excitation signal we can find the acoustic pressure signal for specified points in front of the transducer. The cal_hp command is used to calculated those acoustic pressure. Following is an example to find acoustic pressure for a specified point [53]:

Example: For a point (0,0,10cm), we can use the following command-
```
>> [hp, start_time] = calc_hp (piston, [0 0 0.1]);
```

3.3.9 Two-way response

.

The field is not only able to calculate the acoustic pressure field for a given point but also capable to determine the echo (voltage) waveform return by a point target at a definite spatial location. This is similar to an empirical case where a small rigid sphere (radius $<< \lambda$) is placed into a fluid, pulsing the transducer and estimate the echo. To do this calculation of response calc_hhp command is used. Due to the involvement of both the transmission and reception acoustic pulse, the command takes two transducer handles for the simulation, one for transmit and another one is for receive. A single transducer handle may use for both the transmission and reception, or one may use two different transducer handles for two different cases [53].

3.3.10 Imaging

The most effective application of the field program is the simulation of ultrasound imaging. The main command uses to estimates the echo signal from a collection of scatterers I the calc_scat command. The total imaging processes can be simulated by either the steering the beams or by moving the scatterers, including dynamic aperture, focusing and other effects [53].

CHAPTER 4
Modeling and Simulation of the Tissue Mimicking Phantom

4.1 Finite Element Model of the Tissue Mimicking Phantom

A homogeneous 2-D tissue phantom was constructed using a Finite Element Model software package called ANSYS (ANSYS Inc., Canonsburg). For simulation, we have set the model as a linear, elastic and isotropic with a dimension of $20mm \times 20mm$ square phantom having a circular hard inclusion of diameter $10mm$ against a regular soft background. The square mimics the soft tissue and the circular hard inclusion mimics the tumor tissue placing in the surrounding soft tissues. The material densities for the soft and hard tissue were chosen as $1050\ kgm^{-3}$ & $1500\ kgm^{-3}$ respectively. The Poisson's ratio for both the soft and hard tissue was set as 0.495 [7]. The sketching and the geometric model of the phantom is given below-
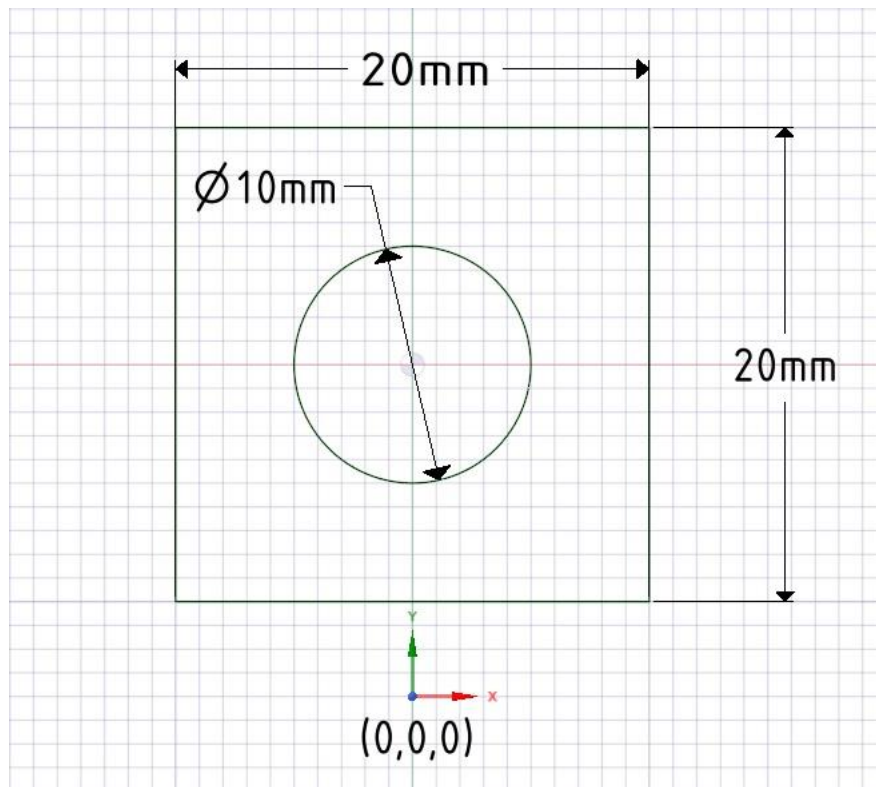

Figure 4.1: 2D sketching of the synthetic Phantom.
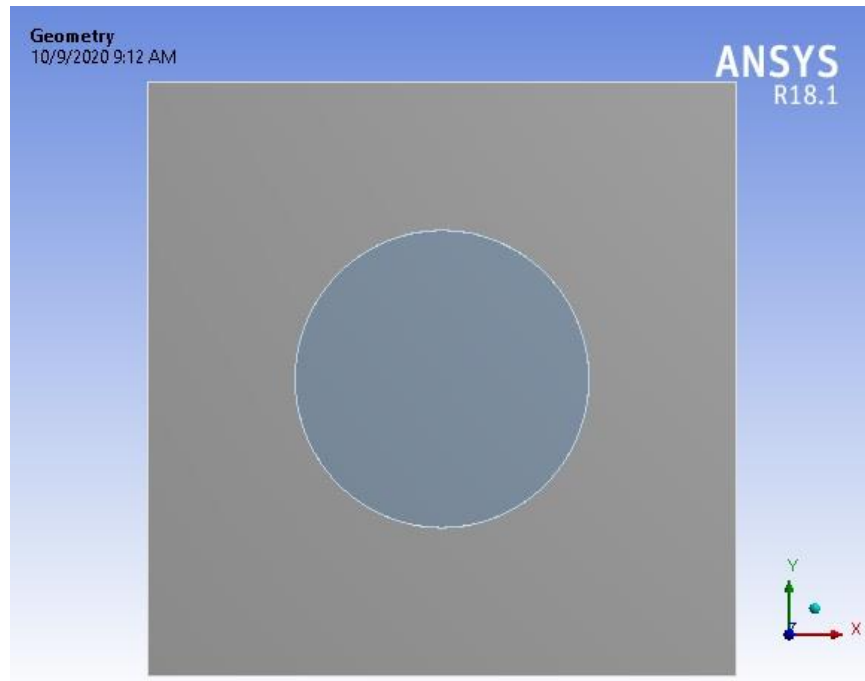
Figure 4.2: Geometric model of the synthetic phantom.

4.1.1 Meshing of the Phantom Model

The model was meshed using triangular method in ANSYS design modeler. The total number of nodes and elements generated was 2049 and 3820. As the tumor is basically more compact than the benign tissue that's why the element size of the malignant tissue (0.75 mm) was kept 3 times denser than the benign one (0.25 mm). The meshing of the phantom is as follow-
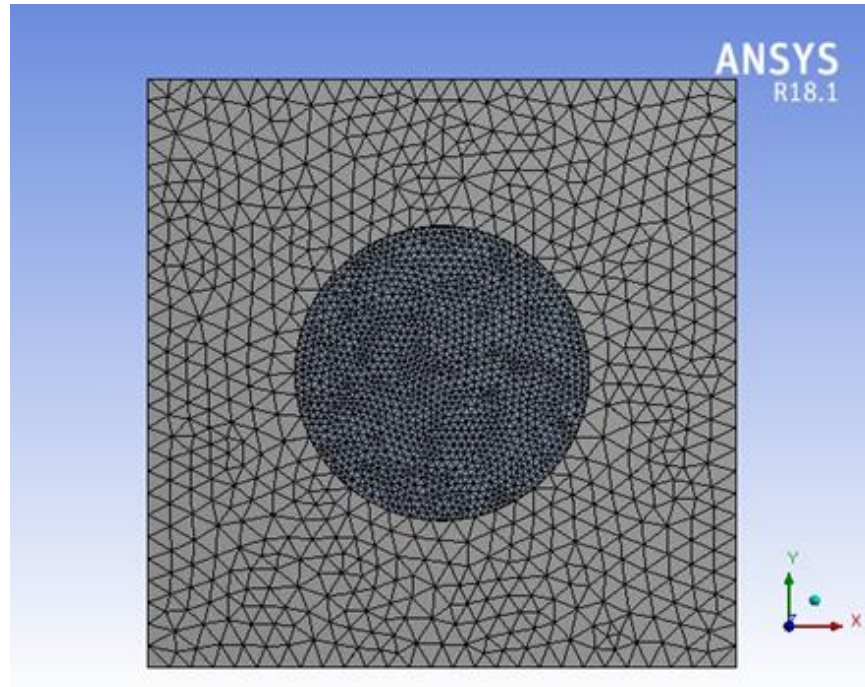
Figure 4.3: Meshing of the geometric model of the synthetic phantom.

4.1.2 Boundary Condition for the Simulation

For the first simulation, the Young's Modulus of inclusion was set to 4 times harder than the soft tissue (40 kPa and 10 kPa respectively). For latter simulation it was 8 times harder (80 kPa and 10 kPa respectively). It was also simulated for same properties contains by both the benign and malignant tissues. For this FEM simulation the top surface of the model was kept fixed, the sides of the model were set free to move while the bottom surface of the model was disturbed by a boundary condition. In this simulation the boundary condition was set as displacement which was 2% of the model height (0.4 mm).
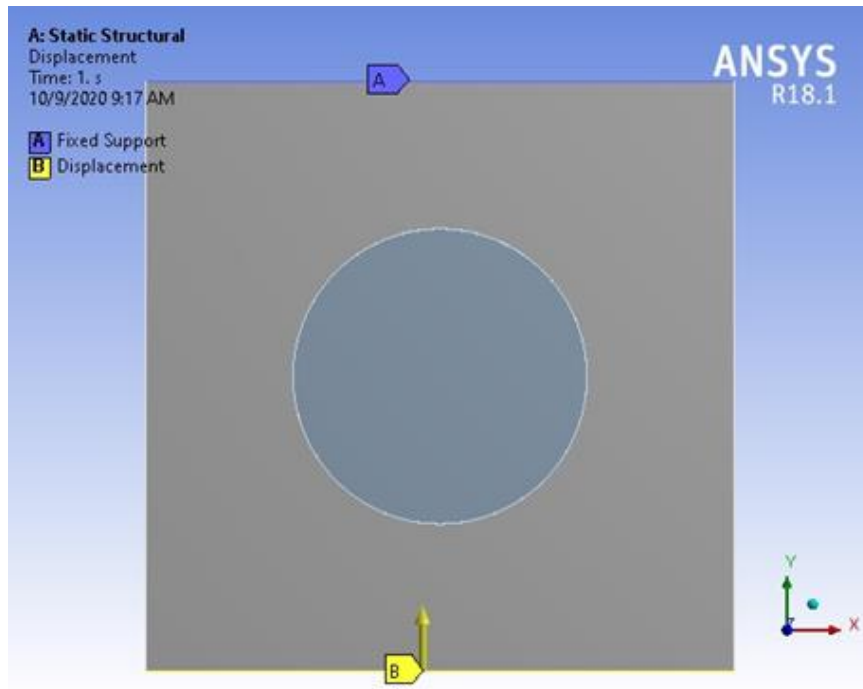
Figure 4.4: Boundary condition (displacement) for the synthetic model (for both 40 kPa and

80 kPa inclusion).

4.2 Simulation of the Phantom

The model was simulated for both the horizontal and vertical axes subjected to the applied displacement. The horizontal axis gives the x-axis directional deformation and the vertical axis simulation gives the y-axis directional deformation. The model was also simulated for total deformation of the phantom and the total strain experienced by the phantom. The displacement map was exported from the design modeler for further simulation.

4..2.1 Directional Deformation (Y axis)

The simulation for the Y-axis deformation was conducted by applying a displacement boundary condition with the value of 0.4 mm along the positive y -axis direction. The top of the phantom was kept fixed for this simulation. The corresponding images of the y-axis deformation for the 10 kPa (which is same as the benign tissue), 40 kPa and 80 kPa backgrounds are given below-

Figure 4.5: Directional Deformation (Y Axis) for same property contained inclusion as the background.

Figure 4.6: Directional Deformation (Y Axis) for 40 kPa inclusion.

Figure 4.7: Directional Deformation (Y Axis) for 80 kPa inclusion.

As we can observe from the above three images that the maximum y-axis deformation (0.4 mm) is at the bottom of the phantom and the minimum y-axis deformation (0 mm) is at the top of the phantom. The above observation was expected because the displacement was applied at the bottom and the amount of displacement is faded out as it goes deeper into the phantom.

4.2.2 Directional Deformation (X axis)

The simulation for the X-axis deformation was conducted by applying a displacement boundary condition with the value of 0.4 mm along the positive y -axis direction. The top of the phantom was kept fixed for this simulation. The sides of the phantom were kept free to move along the x-axis direction. The corresponding images of the x-axis deformation for the 10 kPa (which is same as the benign tissue), 40 kPa and 80 kPa backgrounds are given below-
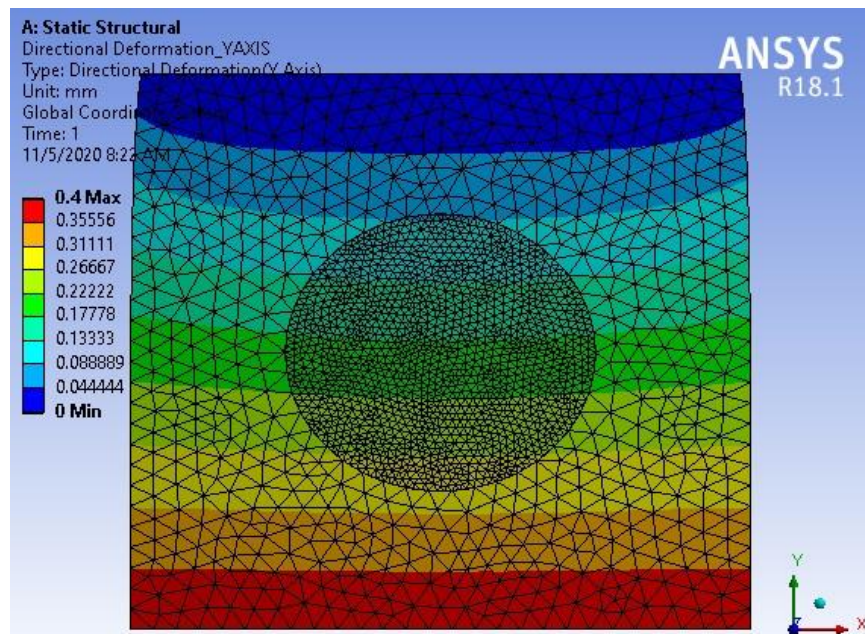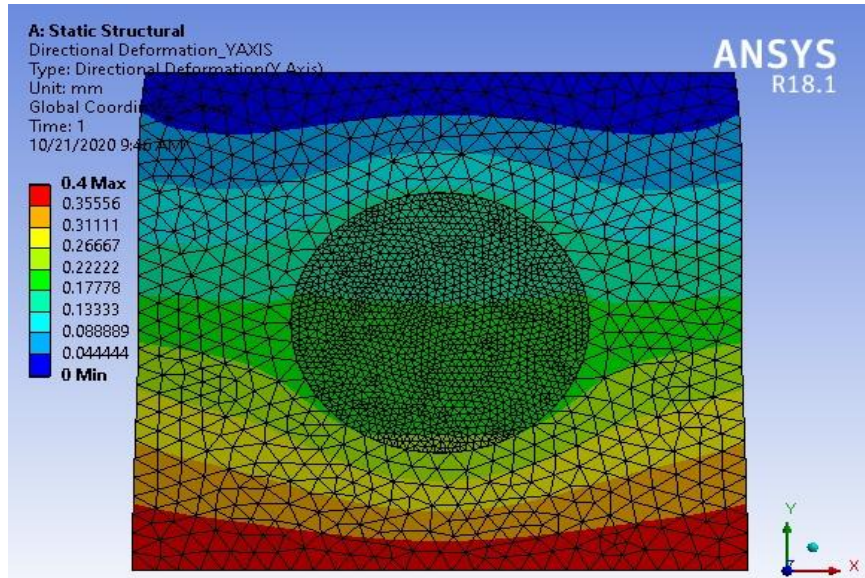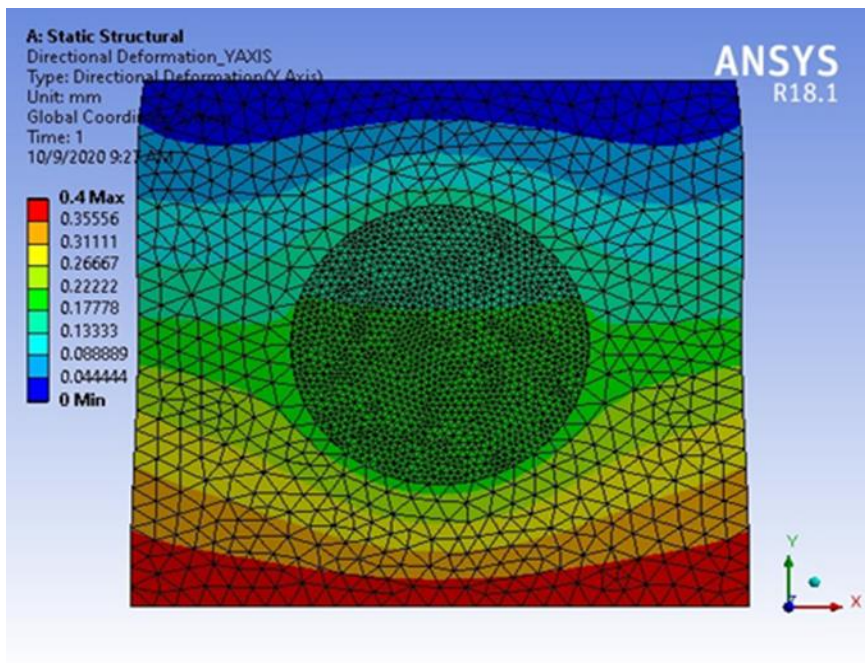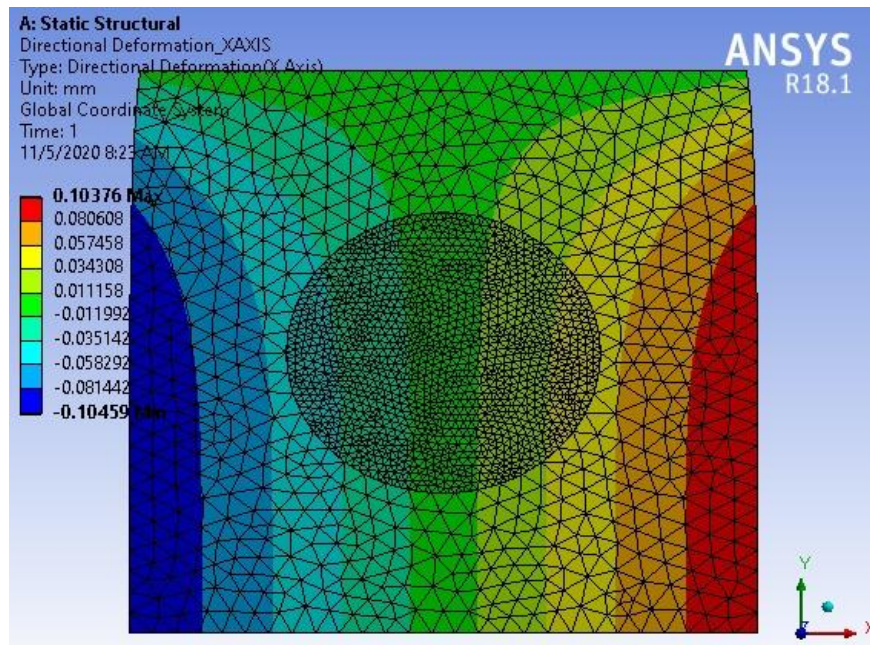

Figure 4.8: Directional Deformation (X Axis) for same property contained inclusion as the background.
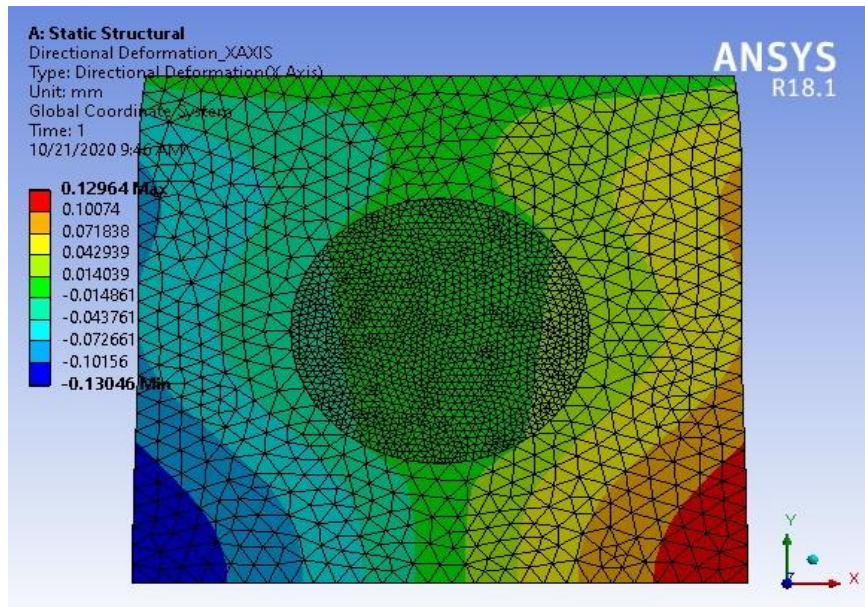
Figure 4.9: Directional Deformation (X Axis) for 40 kPa inclusion.

Figure 4.10: Directional Deformation (X Axis) for 80 kPa inclusion.

We can see from the above three images that the maximum x-axis deformation occurs in both positive and negative sides of the x-axis at the bottom of the phantom. The above observation was expected because the displacement was applied at the bottom of the phantom and the two sides of the phantom were set free to move along both directions of x-axis. Here, one shouldn't be confused with the different colors of the maximum values. The colors were different because in one direction the displacement was positively maximum and in other direction it is negatively maximum. We can observe it from the sketching of the phantom.

4.2.3 Total Deformation

The total deformation is the combine deformation considering both the lateral and axial deformation of the phantom. The simulation for the total deformation of the synthetic phantom was conducted by the same procedure as mentioned above for the both axes. The corresponding images of the total deformation for the 10 kPa (which is same as the benign tissue), 40 kPa and 80 kPa backgrounds are given below-
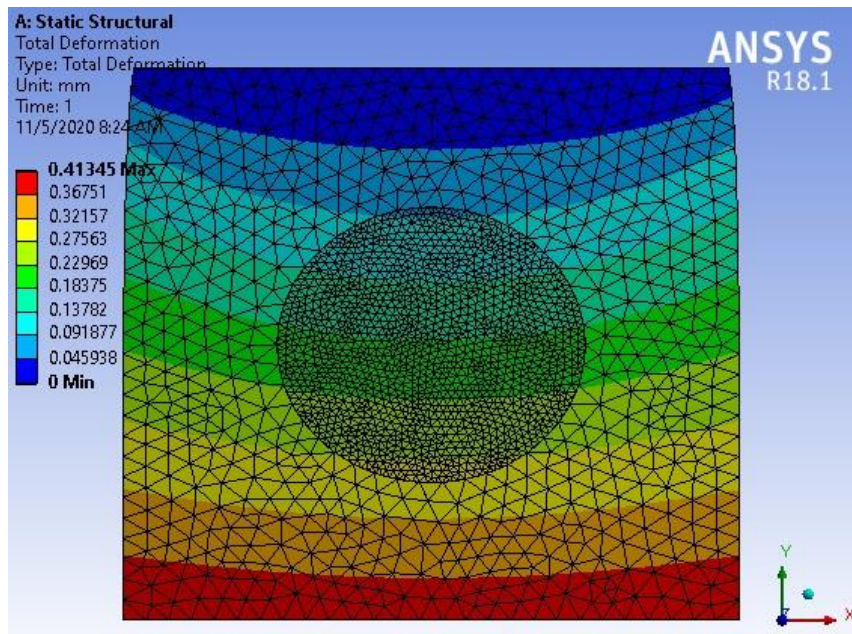
Figure 4.11: Total Deformation for same property contained inclusion as the background.
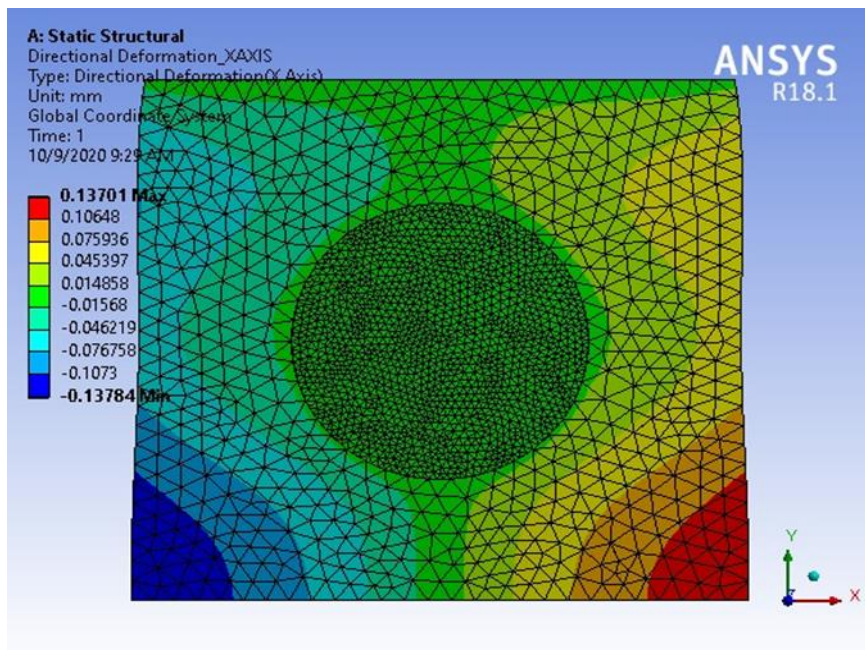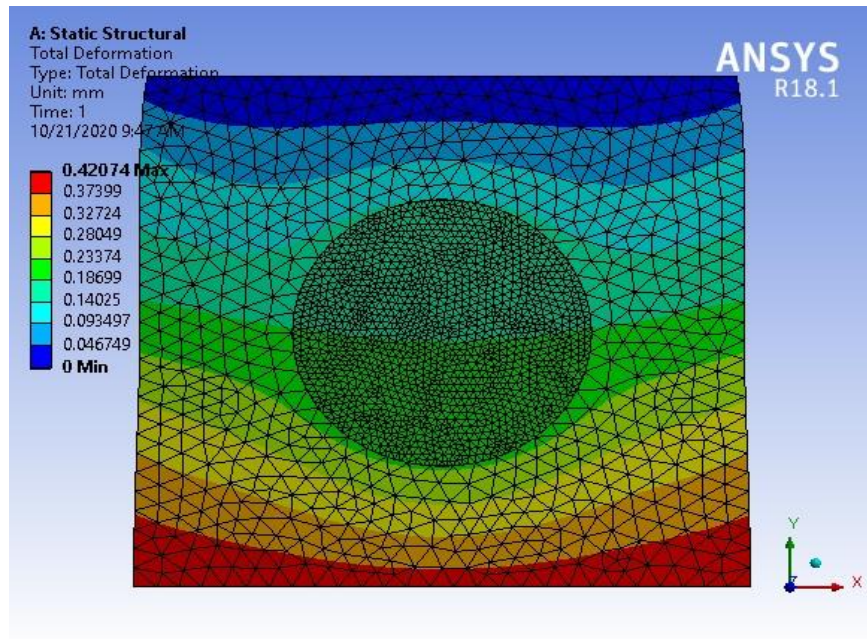
Figure 4.12: Total Deformation for 40 kPa inclusion.
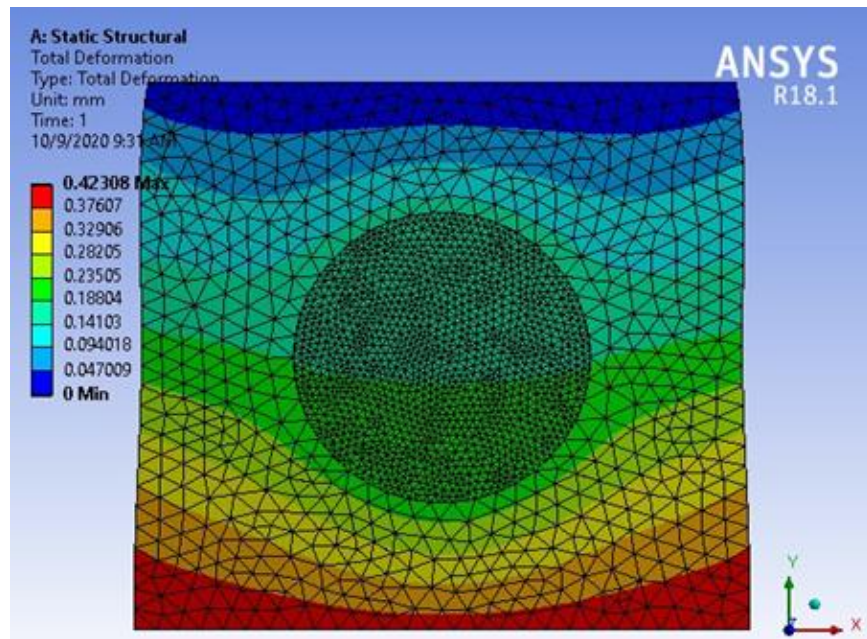
Figure 4.13: Total Deformation for 80 kPa inclusion.

It can be clearly observed from the above images that the total deformation for all the phantoms having an inclusion 10 kPa, 40 kPa and 80 kPa consecutively are maximum at the bottom of the phantom. This result was expected because the maximum deformation of both the phantoms were at the bottom of the phantom.

4.3 Strain Images of the Phantom

The simulation for the total equivalent strain was conducted by applying a displacement boundary condition with the value of 0.4 mm along the positive y -axis direction. The top of the phantom was kept fixed for this simulation. The sides of the phantom were kept free to move along the x-axis direction. The corresponding images of the strain images for the 10 kPa (which is same as the benign tissue), 40 kPa and 80 kPa backgrounds are given below-

Figure 4.14: Strain image of the phantom for same property contained inclusion as the background.
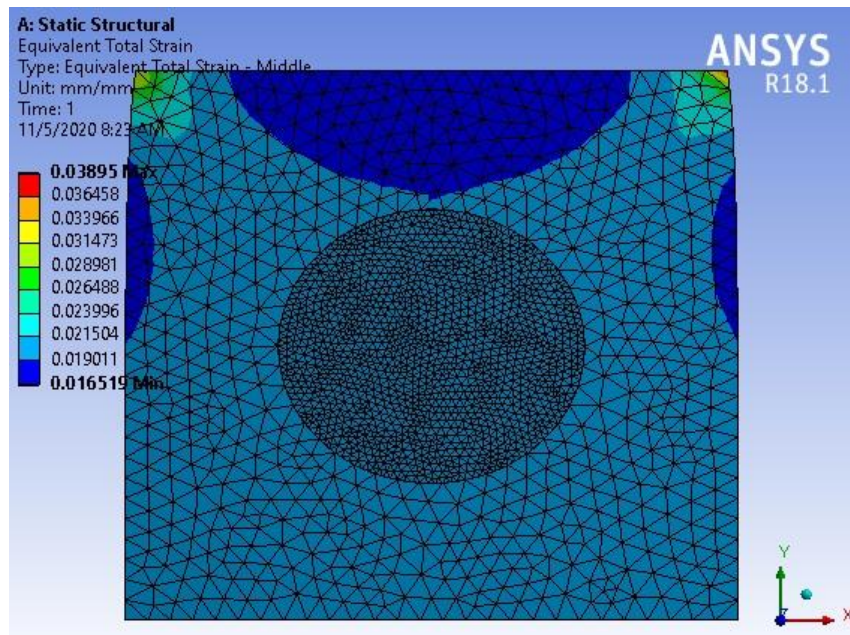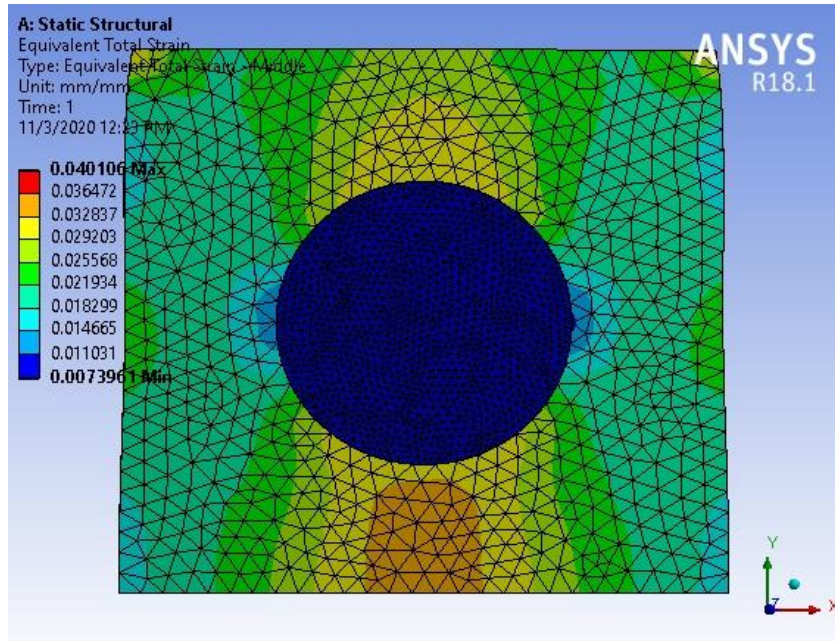
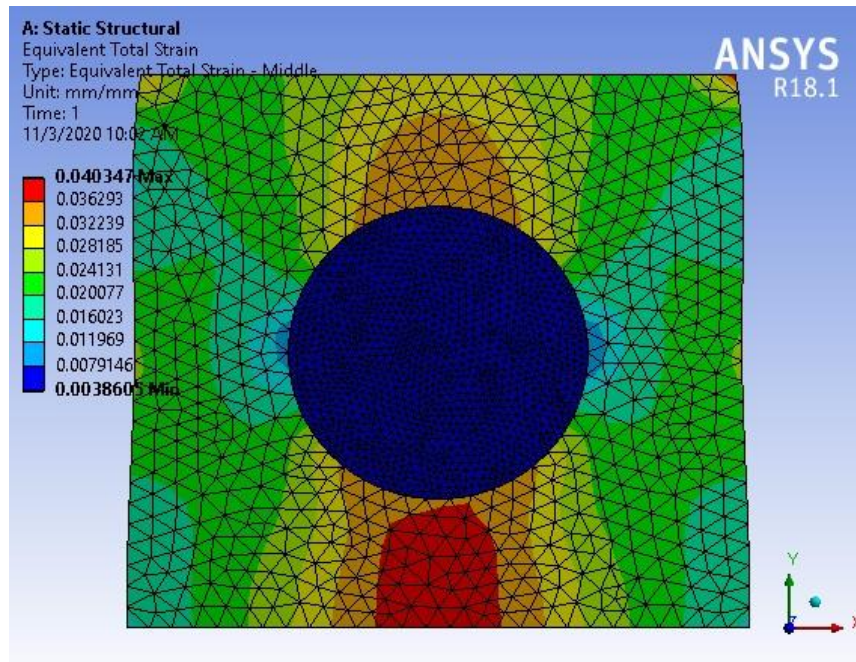Figure 4.15: Strain image of the synthetic phantom for 40 kPa.

Figure 4.16: Strain image of the synthetic phantom for 80 kPa.

We know that strain is the measure of how much an object is stretched or deformed with respect to its original form. Strain is basically deal with the change in length of the object. Strain occurs subjected to the applied force on the object. In this case, we actually take displacement rather than force as the boundary condition. We can clearly see from the above images that the simulations show the expected results. For the same inclusion and background, the strain is same all over the phantom because both the inclusion and background have the same tissue property, so, the change in length for almost every point is same so the strain. For 40 kPa inclusion, the strain of the inclusion is minimum because its young's modulus and density is higher than the background so the change in displacement is also minimum. For 80 kPa inclusion, its explanation is same as that of 40 kPa inclusion.

4.4 Simulation for Ultrasound RF signal

The pre- and post-compression RF signal can be generated using an ultrasound simulation software called FIELD II [54]. The FIELD II ultrasound program basically uses the concept of spatial impulse responses as developed by Tuphllme and Stepanishenin in a series of papers. The simulation of this program is applicable only to linear systems theory to find the ultrasound field for both the pulsed and continuous wave case and does not take into account multiple scattering, reverberations etc. When the transducer is excited by a Dirac Delta function, the spatial impulse response gives the emitted ultrasound field at a specific point in space as function of time. Then the US field could be found by just convolving the spatial impulse response with the excitation signal. The achieved impulse response varies as a function of position relative to the transducer. The total received response in pulse can be found by convolving the transducer excitation function with the spatial impulse response of the emitting aperture. The spatial impulse response of the receiving aperture and the electromechanical transfer function of the transducer yields the received voltage trace.

A typical field simulation is as follows:

- Define transducer type and create transducer
- Define electromechanical impulse response

- Define excitation signal

- Set initial scatterer and beam positions

- Calculate the echo signal

- Move the beam and/or scatterers to next position and repeat

By following the above field calculation procedure, we can generate the RF signal for both the pre- and post-compression data exported from the FEM simulation.

In our FIELD II simulation, we set the following parameters to calculate the RF echo signal:

Parameter	Value	Unit
Speed of Sound	1540	m/s
Transmit center frequency	3	MHz
Transducer element width	0.513	mm
Transducer element height	0.005	mm
Number of Transducer element	128	
Number of active elements	64	
Sampling frequency	100	MHz
Kerf	0.05	mm
Phantom dimension	20*20	mm^2

Table 4.1: Parameters to calculate the RF echo signal.

4.4.1 Ultrasound B-mode Image

B-mode image is a two-dimensional ultrasound image using FIELD II ultrasound simulation program which display bright dots representing the ultrasound pulse echo signal of tissues with different reflection properties. The brightness of each dots represents the amplitude of the returned echo signal. This may allow different visualization and quantification of different

anatomical structures, as well as for the visualization of diagnostic and therapeutic procedures for small animal studies.

Figure 4.17: Pre-compression B-mode image for the phantom having same background and inclusion properties.

Figure 4.18: Post-compression B-mode image for the phantom having same background and inclusion properties.

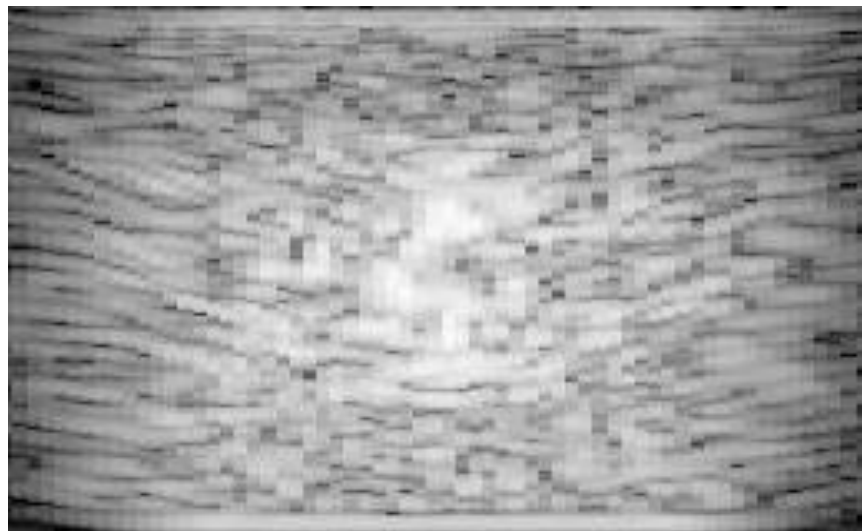Figure 4.19: Pre-compression B-mode image for the phantom having inclusion of 40 kPa.

Figure 4.20: Post-compression B-mode image for the phantom having inclusion of 40 kPa.
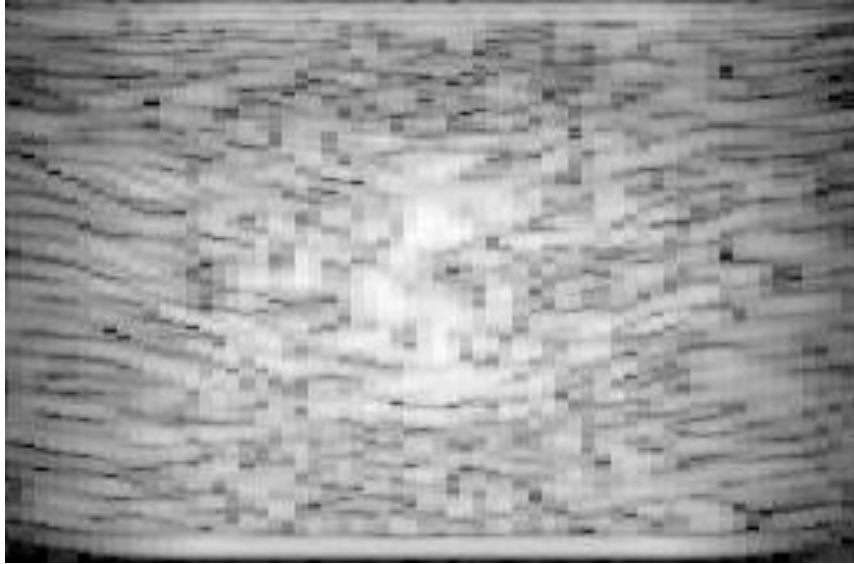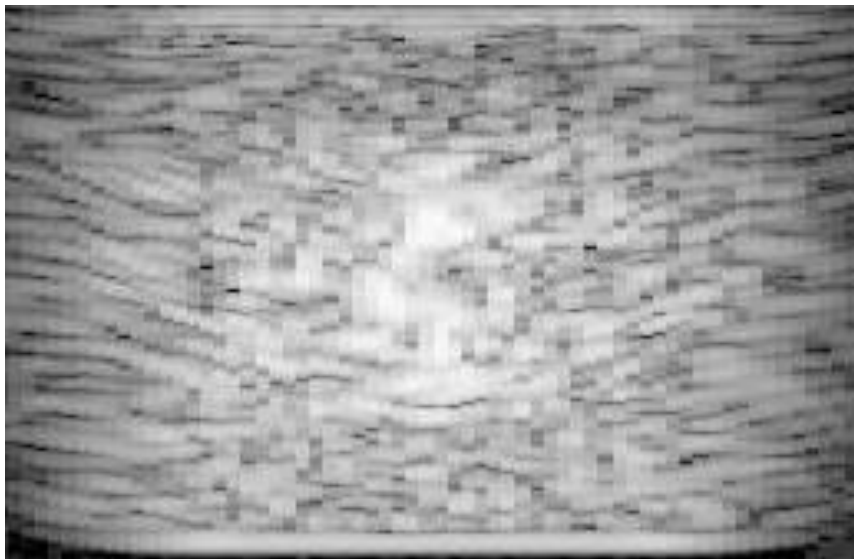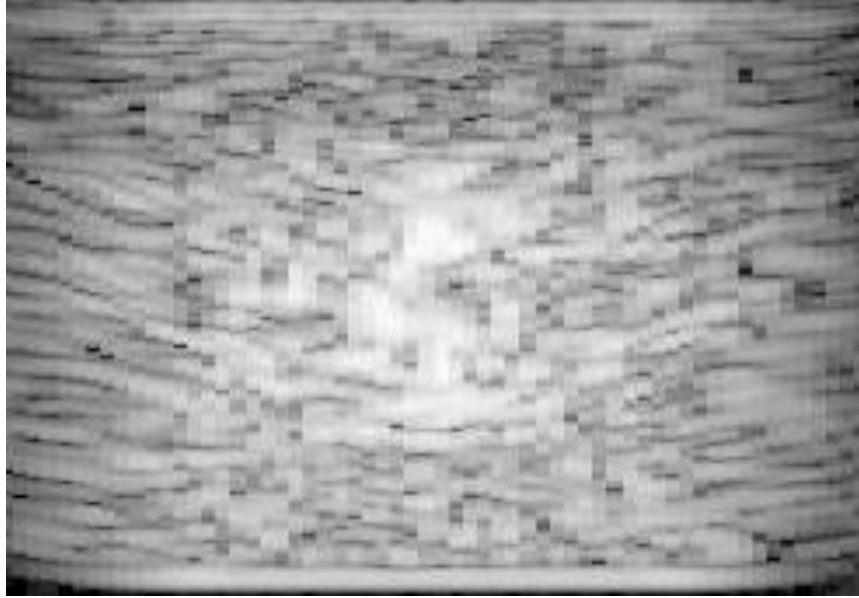
Figure 4.21: Pre-compression B-mode image for the phantom having inclusion of 80 kPa.
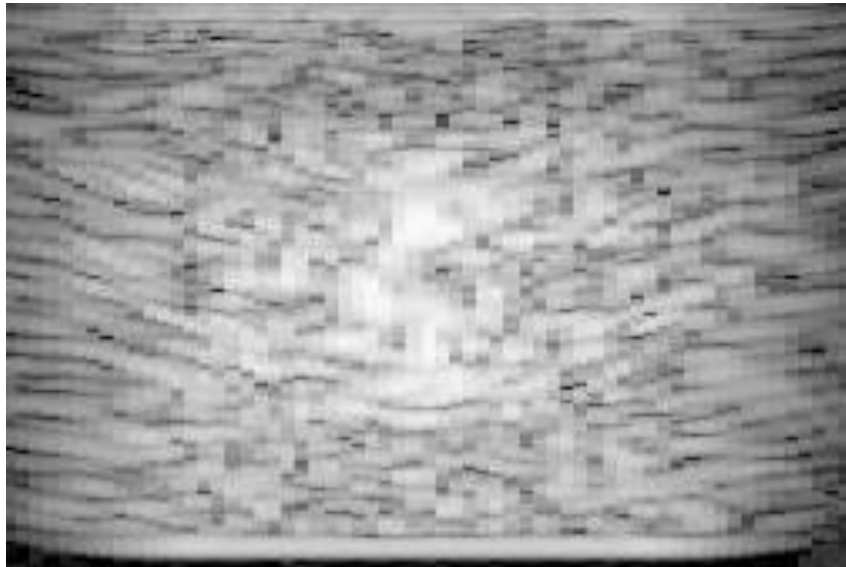

Figure 4.22: Post-compression B-mode image for the phantom having inclusion of 80 kPa.

CHAPTER 5
RESULT AND DISCUSSION

5.1 Introduction to Result and Discussion

The main purpose of this thesis work is to propose an imaging technique which introduce a new time delay estimation algorithm and to reduce the cost of computation of elastography. To do this task as we already mention that a $20mm \times 20mm$ square phantom is constructed with randomly located 2000 scatterers inside it having an inclusion which is circular in shape with a radius of $10mm$. The phantom was then simulated for a displacement boundary condition which was 2% of the height of the phantom using FEM simulator ANSYS. The simulation was simulated for different tissue properties for both the background and inclusion to verify the fact that whether the proposed method actually works or not. For the ultrasound simulation, ultrasound simulation software named FIELD II is introduced. The FIELD II program is used, because it provides good modeling of transducer properties. The program also gives us good modeling of the beam focusing, wave focusing and interactions. In FIELD II, a linear array transducer probe having a center frequency of 3.5 MHz, and sampling rate of 100 MHz was designed. The simulation was performed for 128 RF lines using 64 active transducers firing at a time focusing to a depth to cover the entire phantom. In this thesis work, 2D cross-correlation time delay estimation technique is used which actually returns the cross-correlation of two pre- and post-compression RF echoes. This cross-correlation measures the similarity between the pre- and post-compression data as a function of the lag. Another objective of this thesis is whether we could make an imaging technique which is less computationally costly or not. To make this imaging less costly we skip the procedure to estimate the strain from the above attained delays. Rather MATLAB surf tool is used to visualize the matching scatterers which shows us the region where the scatterers are best match after compression which indicates that the scatterers at these points are less displaced. The conventional strain imaging technique and the proposed technique are discussed below.

5.2 Conventional Strain Imaging Technique

Strain imaging technique has gained significance in recent years to diagnosis tumors or cancers. In this technique, an ultrasound probe is used to deform tissue over the region of interest by applying a mechanical compression. Because of the different tissue stiffness properties different tissue displacements are results with different time shifts in the recorded RF signals. The consecutive rf ultrasound echoes are recorded before and after compression of the phantom. Then a time delay estimation algorithm is used to calculate the delay between pre- and post-compression RF signals. Then the local tissue displacements are estimated from the above time delays whose axial gradient gives the estimated strain [7]. The flow chart to estimate the strain and the imaging is given below-
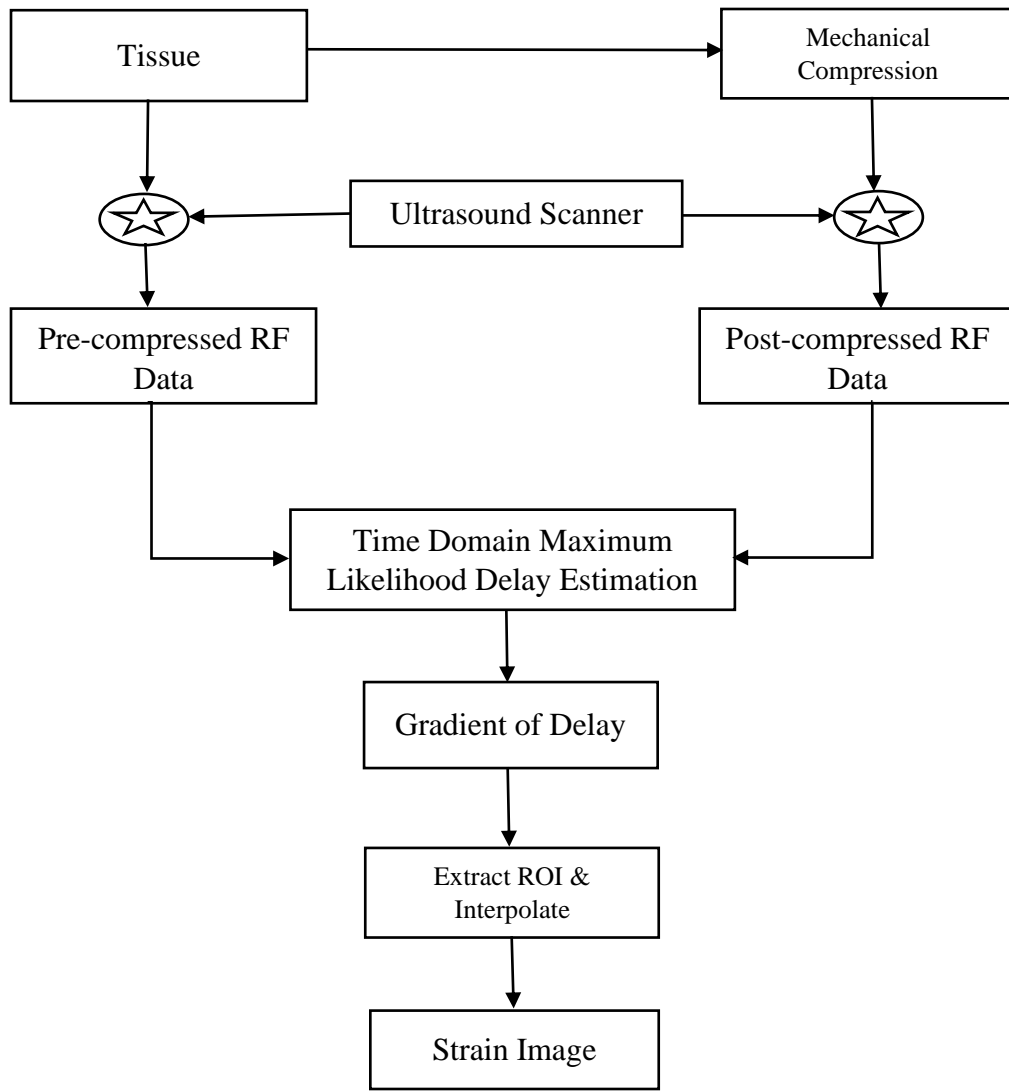
Figure 5.1: Flow chart to estimate the strain and the imaging using conventional technique.

5.3 Proposed Ultrasound Imaging Technique

As mentioned earlier, the main purpose of this thesis work is to introduce a new time delay estimation technique and to design an algorithm which is less computationally costly than estimating the strain imaging. To do this, we follow the same conventional work flow except choosing a 2D cross-correlation technique for estimation of the time delay and used a MATLAB surf tool to visualize the correlation between the pre- and post-compression rf data. The flow chart of the proposed imaging technique is given below-
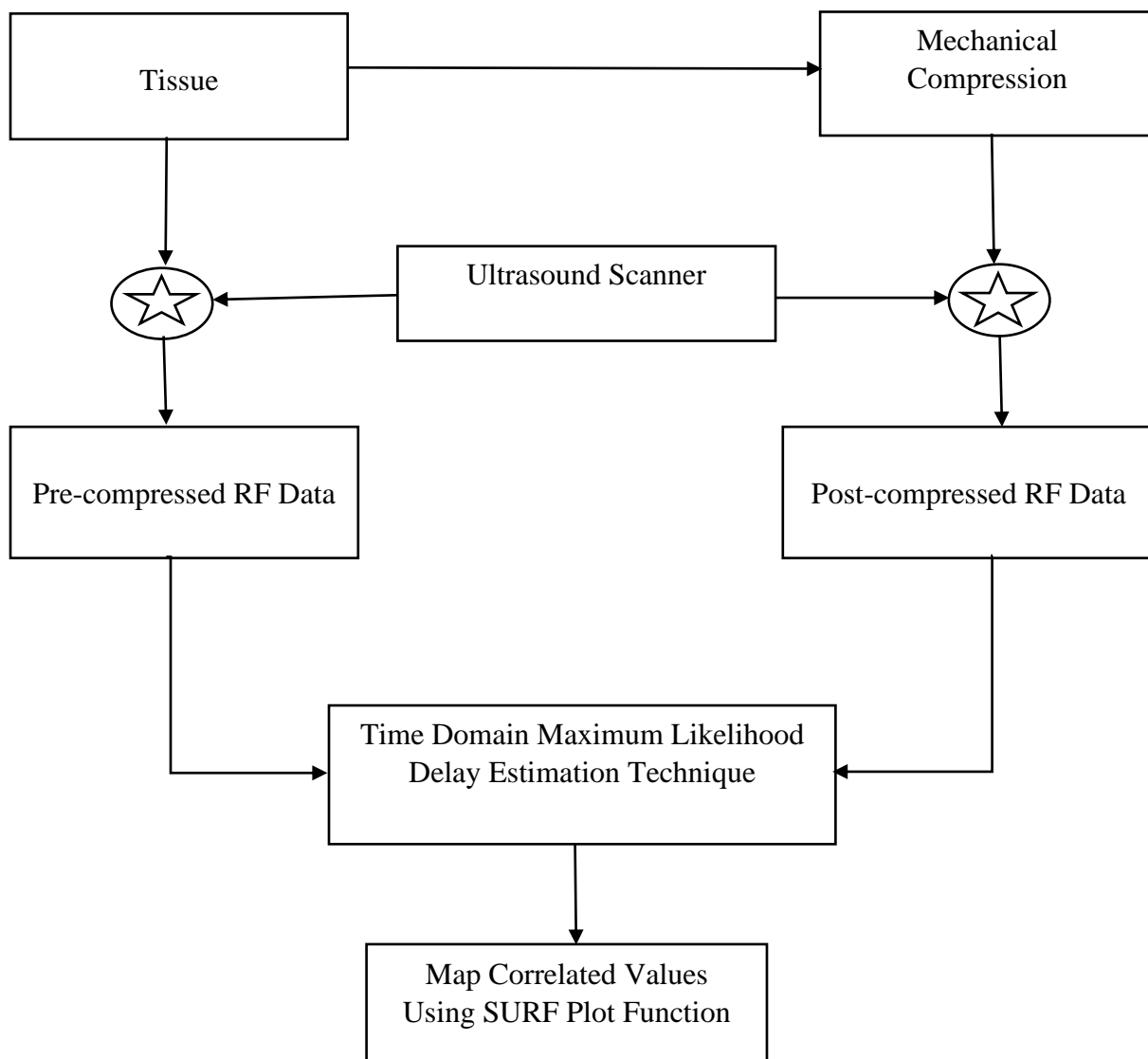
Figure 5.2: Flow chart to ultrasound imaging using the proposed method.

5.3.1 Extraction of correlated values using 2D cross-correlation

Correlation is an operation which is used to measure the degree of similarity between two signals to extract information that depends to a large extent on the application. It is widely recognized and used approach to determine the displacements between two images. So, it can also be used to find feature point displacement between deformed and undeformed images. In this thesis work, the cross-correlation between two signals is estimated by using the xcorr2 command in MATLAB. The xcorr2(X, Y) returns the cross-correlation of matrices X and Y with no scaling. The xcorr2 command is just the two-dimensional version of the MATLAB command xcorr. The 2-D cross-correlation of an M-by-N matrix, X, and a P-by-Q matrix, H, is a matrix, C, of size M+P-1 by N+Q-1. The extracted correlated values for different inclusion properties for all RF lines are given below.

Figure 5.3: Correlation values achieved from pre- and post-compression phantom when the inclusion (10 kPa) is same as the background (10 kPa).

The above figure shows the correlation values obtained from the phantom which has the same inclusion properties as the background. It can be observed from the above figure that as the young's modulus, Poisson ratio, density and other properties are same for both the inclusion and background the correlation values for the entire phantom are almost same. There is a little change of values at the inclusion which could be negligible.
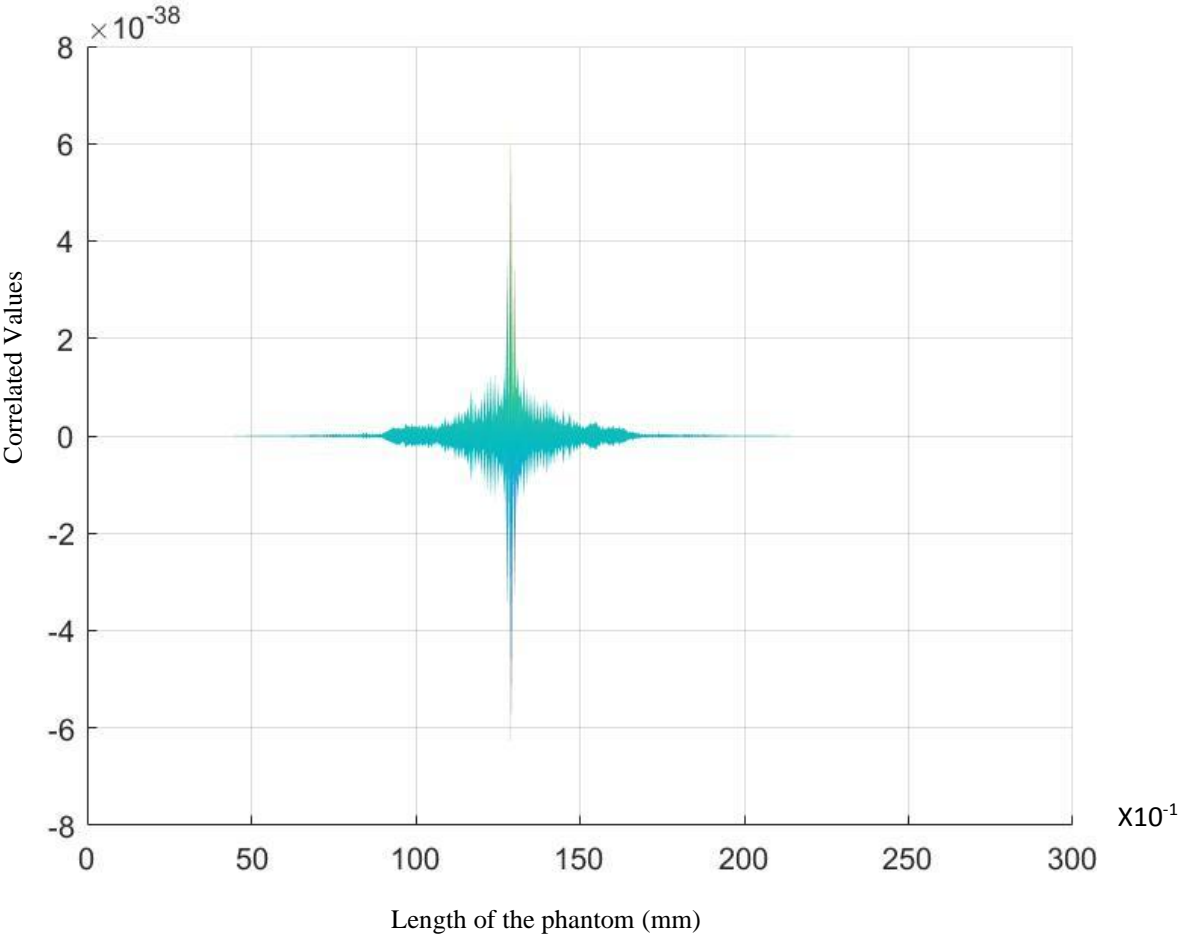
Figure 5.4: Correlation values achieved from pre- and post-compression phantom when the inclusion (40 kPa) is 4 times greater than the background (10 kPa).

The above figure shows the correlation values achieved from pre- and post-compression phantom when the inclusion (40 kPa) is 4 times greater than the background (10 kPa) in terms of young's modulus. The Poisson ratio is same for both the inclusion and background but the density is different for the inclusion and background. From the above figure it is clearly

noticeable that there is huge difference between the correlated values of the inclusion and background which indicates the differentiation between cancerous tissue and benign tissue.

Figure 5.5: Correlation values achieved from pre- and post-compression phantom when the inclusion (80 kPa) is 8 times greater than the background (10 kPa).

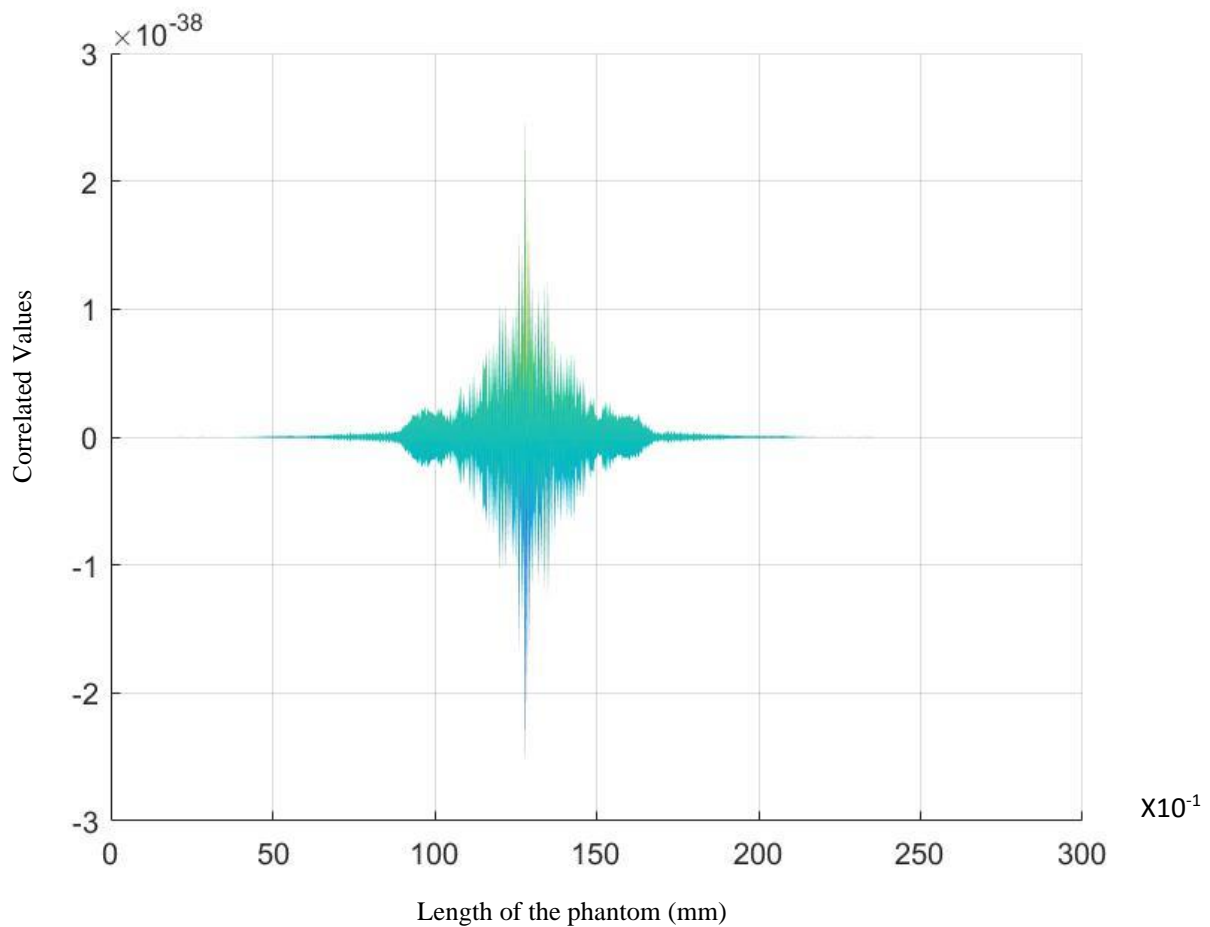The above figure shows the correlation values achieved from pre- and post-compression phantom when the inclusion (80 kPa) is 8 times greater than the background (10 kPa) in terms of young's modulus. The Poisson ratio is same for both the inclusion and background but the density is different for the inclusion and background. From the above figure it is clearly noticeable that there is huge difference between the correlated values of the inclusion and background which indicates the differentiation between cancerous tissue and benign tissue. The

basic difference between the 8 times and 4 times inclusion is that the correlated values at the inclusion is higher for 8 times harder inclusion which was expected.

5.3.2 Mapping of Correlated Values

In this thesis work it is tried to make an imaging technique which is less computationally costly from the pre- and post-compression RF echo signals. To make this imaging less costly we use MATLAB surf tool to visualize the matching individual RF sample which shows us the region where the individual RF sample are best match after compression which indicates that the scatterers at these points are less displaced. The mapping of correlated values for different inclusion properties are given below.
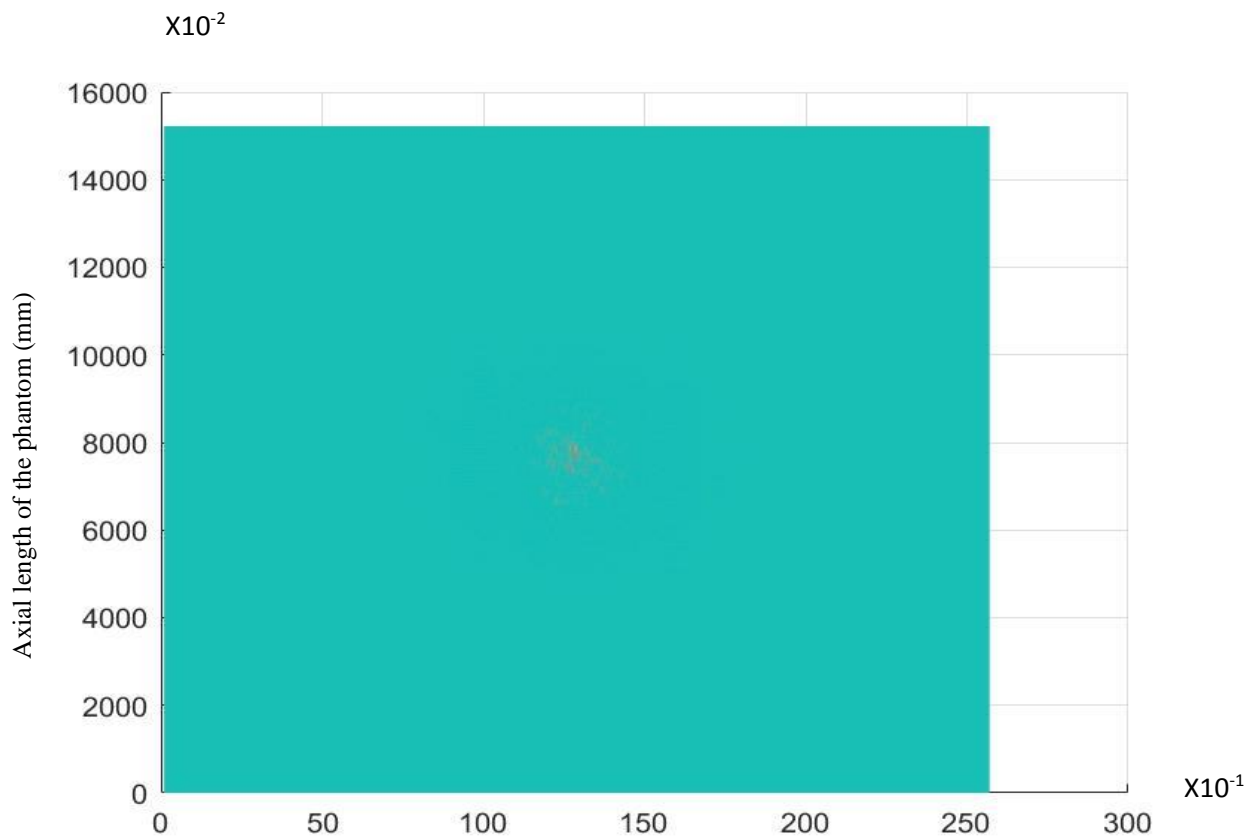
Figure 5.6: Mapping of correl Lateral length of the phantom (mm)   nd post-compression phantom when the inclusion (10 kPa) is same as the background (10 kPa).

The above image shows the mapping of correlated RF echo signal values obtained from pre- and post-compression phantom when the hardness of the inclusion of the phantom is same as that of the background of the phantom. As the young's modulus for both the inclusion and the background are same, the displacement of the scatterers decreases as it goes deeper to the phantom. So, maximum number of scatterers displaced from its original location which indicates a few numbers of scatterers shows best matching results. Due that reason we can observe from the above image that the inclusion is not clearly distinguishable from the background. That means we may say that there is no differentiable malignant tissue in the phantom. Theoretically the inclusion and background should not 100% distinguishable. But due to rounding off the received RF data some data are lost and hence makes a little bit noise.

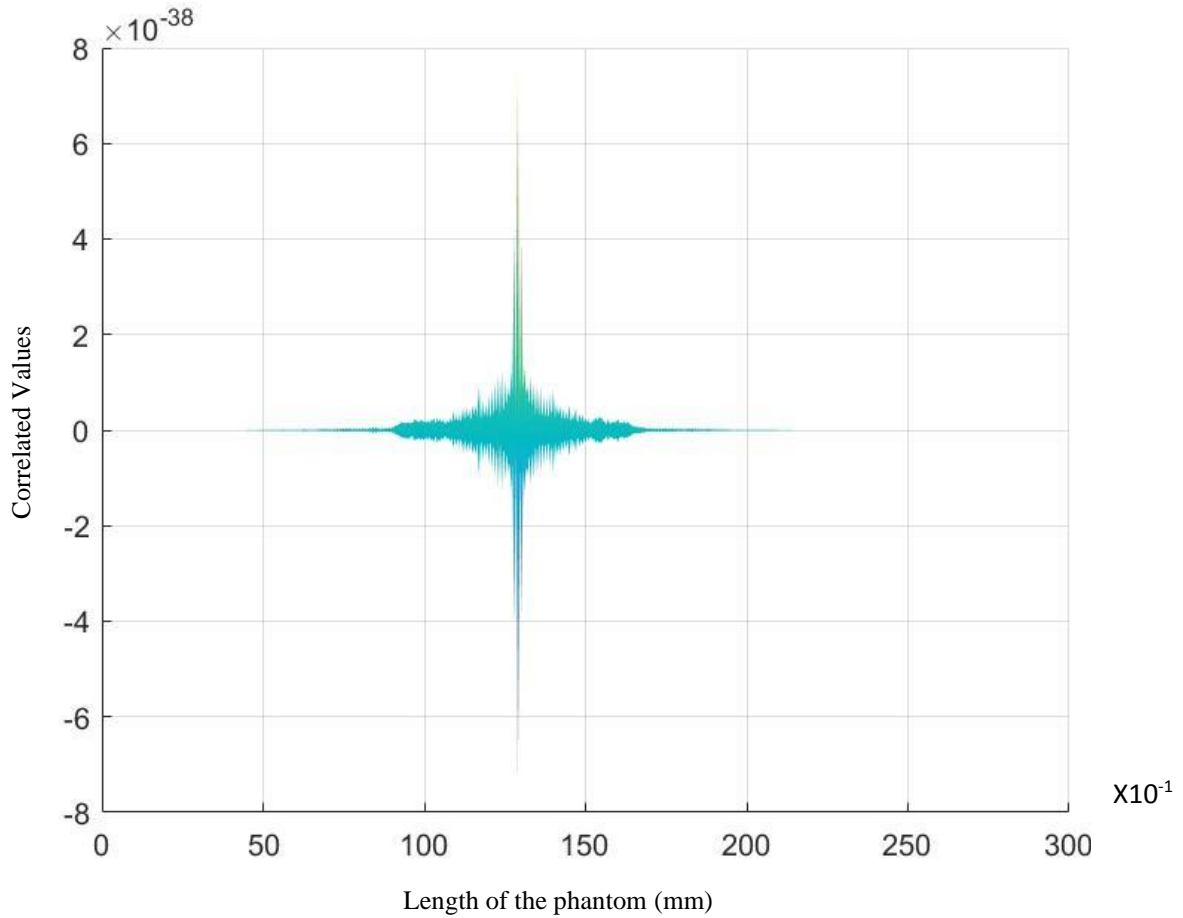Figure 5.7: Mapping of correlation values achieved from pre- and post-compression phantom when the inclusion (40 kPa) is 4 times harder as the background (10 kPa).

The above image shows the mapping of correlated RF echo signal values obtained from pre- and post-compression phantom when the hardness of the inclusion of the phantom is 4 times as that of the background of the phantom. As the young's modulus of the inclusion is 4 times larger than the background, the displacement of the scatterers after compression is less in the inclusion than the background of the phantom. So, when we take the correlated values of the pre- and post-compression RF echo signal using the xcorr2 MATLAB function the scatterers of the inclusion shows the best matching results. Due that reason we can observe from the above image that the inclusion is distinguishable from the background. That means we may say that there is a differentiable malignant tissue in the phantom which located at the center of the phantom.
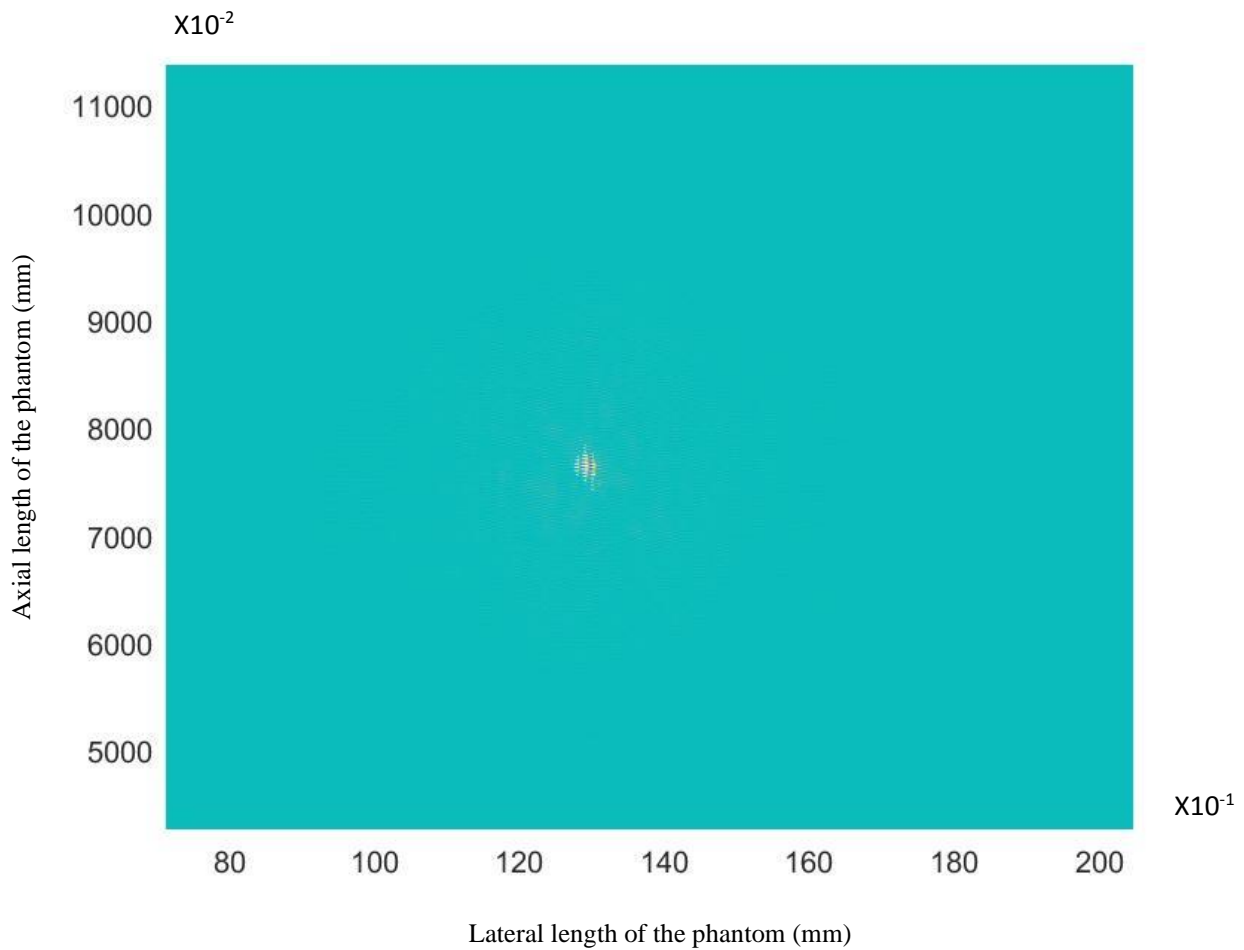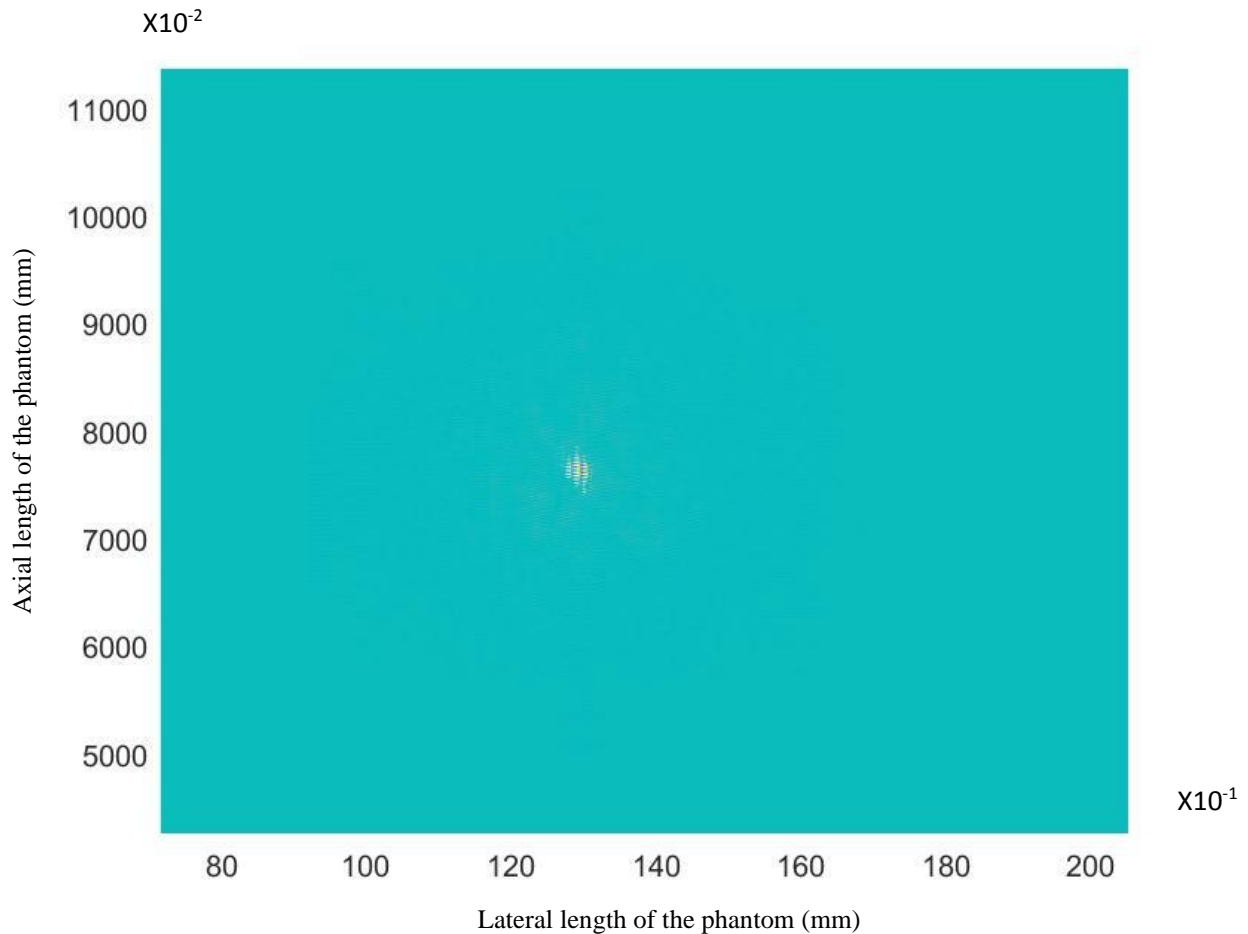

Figure 5.8: Mapping of correlation values achieved from pre- and post-compression phantom when the inclusion (80 kPa) is 8 times harder as the background (10 kPa).

The above image shows the mapping of correlated RF echo signal values obtained from pre- and post-compression phantom when the hardness of the inclusion of the phantom is 8 times as that of the background of the phantom. As the young's modulus of the inclusion is 8 times larger than the background, the displacement of the scatterers after compression is less in the inclusion than the background of the phantom. So, when we take the correlated values of the pre- and post-compression RF echo signal using the xcorr2 MATLAB function the scatterers of the inclusion shows the best matching results. Due that reason we can observe from the above image that the inclusion is distinguishable from the background. That means we may say that there is a differentiable malignant tissue in the phantom which located at the center of the phantom.

5.4 Comparison Between the Conventional Strain Imaging and Proposed Method

The following figure shows the fem model of the phantom for conventional strain imaging technique. In this figure we can see the malignant tissue is right on the middle of the phantom. The goal was to simulate strain imaging from where we can detect the malignant tissue.
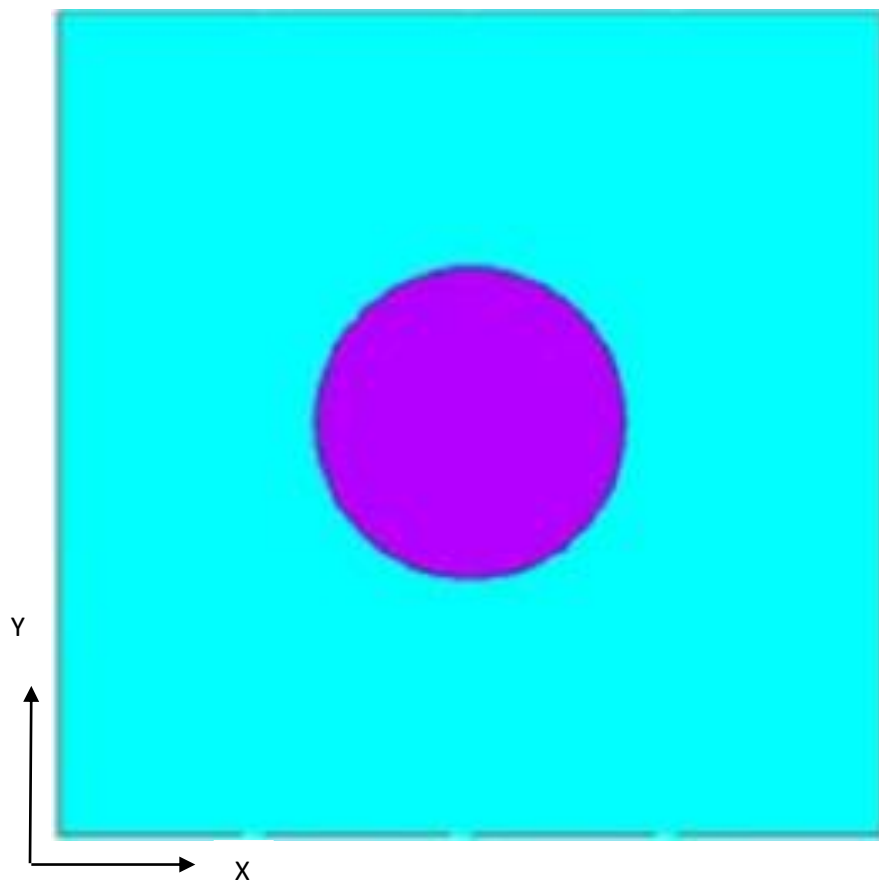
Figure 5.9: FEM model of the phantom for a conventional strain imaging [7].
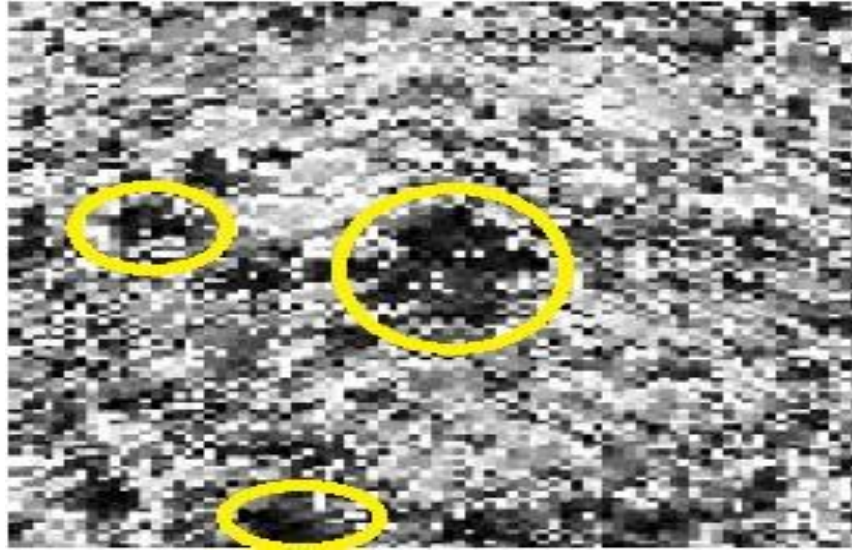
Figure 5.10: Strain Image obtained from conventional cross-correlation without interpolation [7].
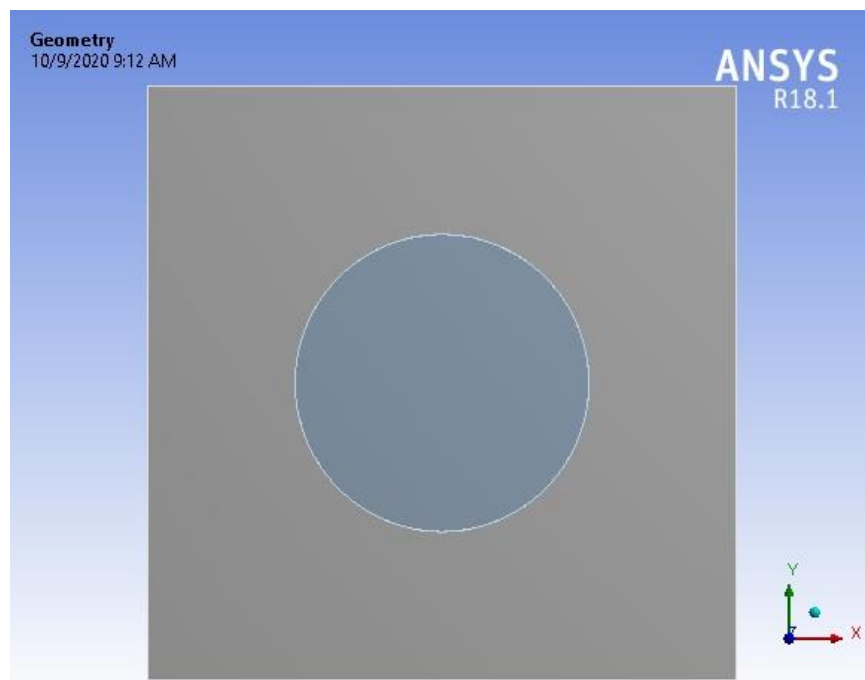
Figure 5.11: FEM model of the phantom for the imaging of the proposed method.
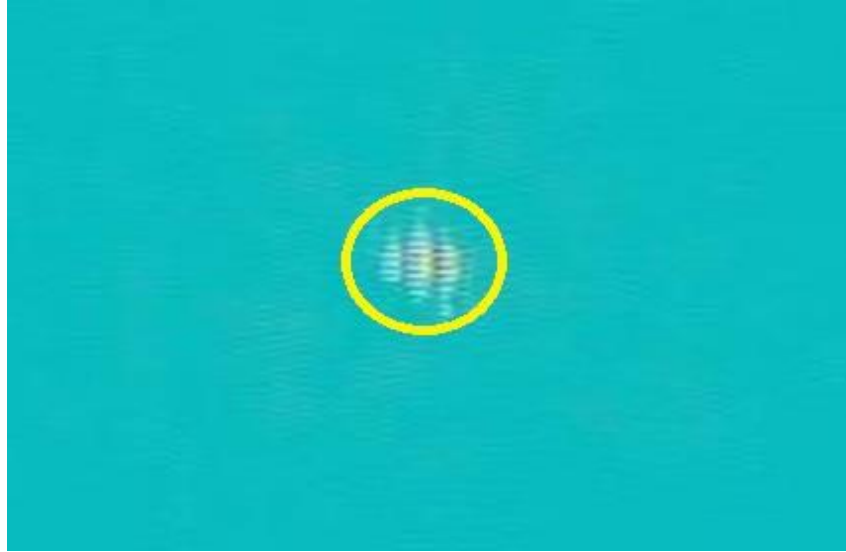
Figure 5.12: Mapping of correlated values when the inclusion's Young's modulus is 4 times larger than background's Young's modulus.

Figure 5.10 shows the strain imaging of the phantom using a conventional cross-correlation algorithm. From this B-mode image we can see that although we can identify a different object (object encircled by large yellow circle) which is different than its surroundings but there are others different objects (objects encircled by small yellow circle) and these objects are different than its surroundings. So, this introduces an ambiguity whether each object represents the malignant tissue or not.

Figure 5.11 shows the fem model of the phantom for the proposed method. In this figure we can see the that the malignant tissue is right on the middle of the phantom which is similar to the figure 5.9. Our aim is to simulate the phantom, find the correlated values and mapped them. Figure 5.12 shows us the mapping of the correlated values where the correlated values are found using 2-D cross-correlation. In this image it could be seen that at the middle of the phantom there is a different object (encircled by yellow circle) which is different form its surroundings. It seems there is no ambiguity to identify which one is malignant tissue as it was in the above discussion. So, it could be concluded that the proposed method is better than the conventional strain imaging method.

5.5 Quantitative Comparison between the Conventional Strain Imaging and Proposed Method

As 2D time delay estimation is better than 1D time delay estimation [68]. Here, we will analyze the comparison between conventional and proposed method using the 2D delay estimation. To compare the proposed method with the conventional strain imaging quantitatively, the elapsed time of each step is calculated using the MATLAB tic toc function. As we already know, every imaging has pre-imaging and post-imaging processes. So, the analysis of the comparison breaks down into two parts.

Based on the above-mentioned procedure, calculated pre-imaging elapsed time (only the pre- and post-compression elapsed time) using 1D time delay estimation exceeded the whole simulation elapsed time of proposed method. So, for the fair comparison, here, 2D time delay estimation elapsed time is calculated for both the methods. The table of the estimated elapsed time for different simulations is given below:

Simulations	Time Elapsed
1D pre compression	95.6088099 seconds
1D post compression	142.494453 seconds
2D pre compression	96.143224 seconds
2D post compression	94.307406 seconds
2D cross correlation	31.574962 seconds
2D surf Mapping	0.046730 seconds
Gradient of delay	0.067423 seconds

Table 5.1: Estimated elapsed time for different simulations.

Now, to compare the methods, we can again draw the flow chart for both methods where each steps contains its elapsed time with itself. To make the comparison more meaningful, at first, we will write the elapsed times in equations.

Let's assume the total time required for execution of the conventional strain imaging is

$Y = S_{pre} + S_{post} + T_{DS} + G_{DS} + E_s + S_s$

Where,

Y = Total elapsed time for the execution of the conventional strain imaging.

S_{pre} = Elapsed time for pre-compression ultrasound simulation of the strain imaging.

S_{post} = Elapsed time for post-compression ultrasound simulation of the strain imaging.

T_{DS} = Elapsed time to find the delay time between pre- and post-compression RF signals for strain imaging.

G_{DS} = Elapsed time to calculate gradient of delay.

E_s = Elapsed time to estimate the strain.

S_s = Elapsed time to done with strain imaging.

Here, $S_{pre} + S_{post} + T_{DS,}$ is the pre-process time of the imaging.

The total time needed for this preprocess time, $S_{pre} + S_{post} + T_{DS} =$ 96.143224 + 94.307406 + 31.574962 = 222.025592 seconds

And, in the post-process imaging, $G_{DS} = 0.067423$ second
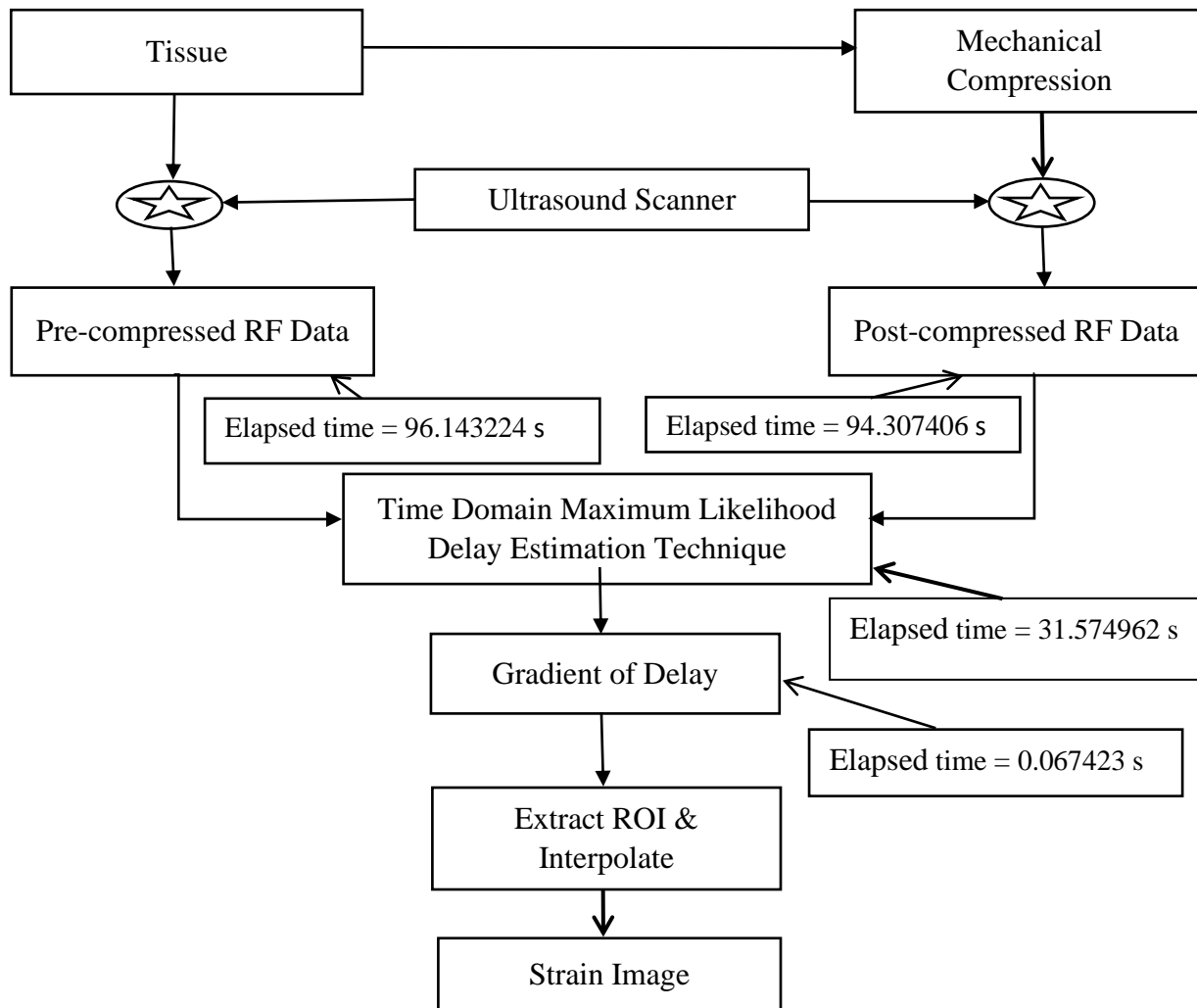
Figure 5.13: Flow chart to estimate the strain and the imaging using conventional technique with elapsed time**.**

Now, by looking at the flow chart of the proposed method, we can write another equation for proposed method.

$X = C_{pre} + C_{post} + T_{DC} + M_c$

Where,

X = Total elapsed time for the execution of the proposed method.

C_{pre} = Elapsed time for pre-compression ultrasound simulation of the proposed method.

C_{post} = Elapsed time for post-compression ultrasound simulation of the proposed method.

T_{DC} = Elapsed time to find the delay time between pre- and post-compression RF signals for proposed method.

M_c = Elapsed time for mapping the correlated values.
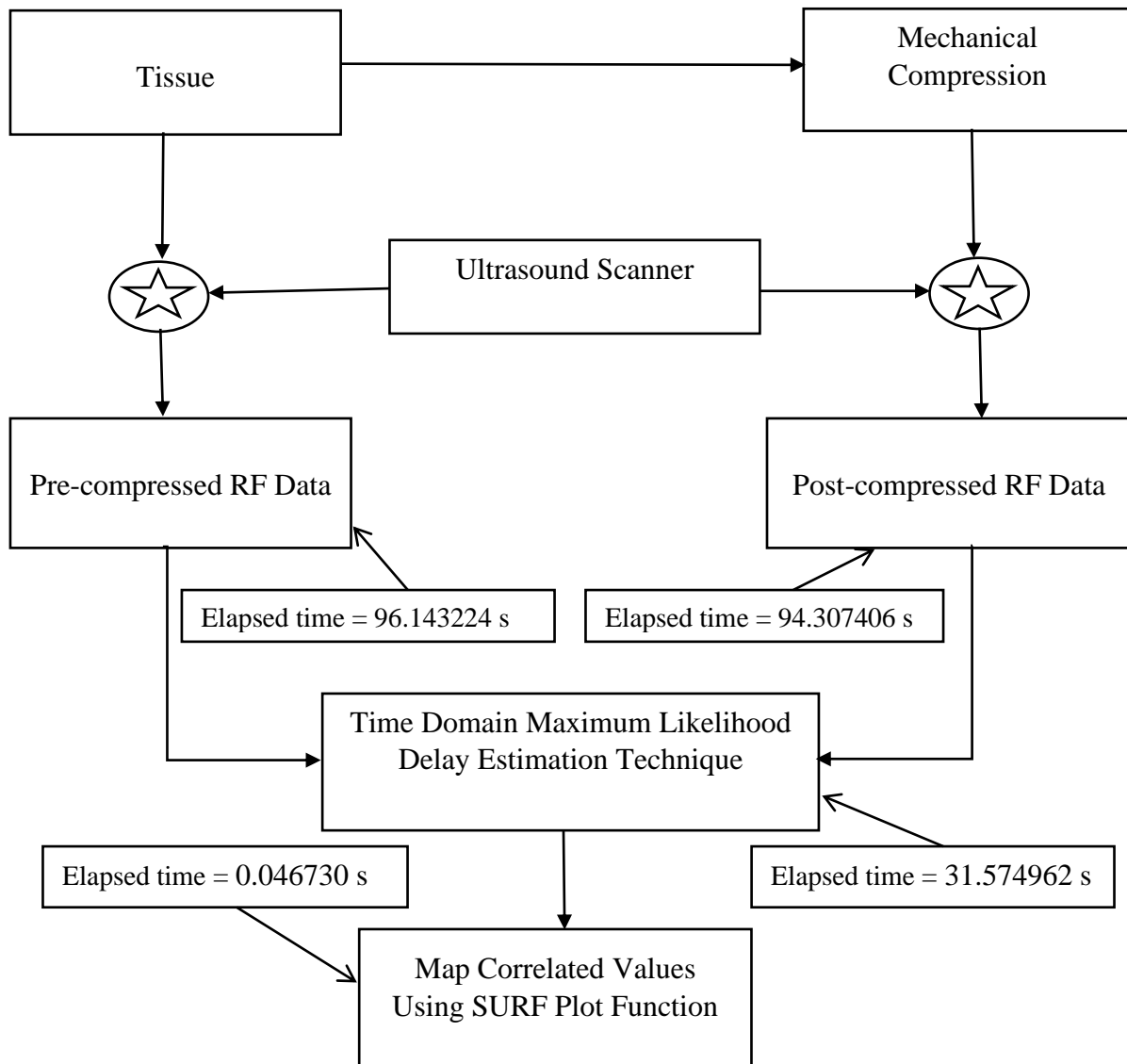
Figure 5.14: Flow chart to ultrasound imaging using the proposed method with elapsed time.

Here, $C_{pre} + C_{post} + T_{DC}$, is the pre-process time of the imaging.

The total time needed for this pre-process, $C_{pre} + C_{post} + T_{DC} = $ 96.143224 + 94.307406 + 31.574962 = 222.025592 seconds.

And, in the post-process imaging, $M_c = 0.046730$ second.

So, from the above information, we can say that , the total imaging time needed for the execution of proposed method, $X = 222.025592 + 0.046730$ seconds and the total time needed for the execution of conventional strain imaging is $Y = 222.025592 + 0.067423 + E_s + S_s$.

Now, in Y the pre-process time and G_{DS} cumulatively exceeded the elapsed time for the whole execution of the proposed method. Also, the $(E_s + S_s)$ is non-zero and non-negative required time which we don't even need to calculate for the comparison. Because, excluding these two elapsed times, we already saw that, Y requires more time than X for execution. So, by considering the above discussion it could be said that the proposed method is less computational costly than conventional strain imaging method.

CHAPTER 6
CONCLUSION AND FUTURE WORK

6.1 Conclusion

The objectives of this thesis work were mainly to introduce a new time delay estimation technique with a new algorithm and to reduce the cost of computation of the imaging. The time delay estimation procedure and then the cost of computation is discussed below.

To estimate the motion as a time delay in sequences of ultrasound echo signals is needed for a wide range of modern ultrasound-based signal processing applications. Time delay estimation lies at the heart of blood flow estimation, tissue velocity estimation [12]-[15], tissue elasticity estimation [8]-[10], acoustic radiation force imaging (ARFI) [55]-[56], and many other applications.

The time-delay estimators are typically classified based on two fields. One is the type of signal which are to be estimated (i.e., envelope signal, radio frequency signal (RF), in-phase, and quadrature signal I/Q etc.) and the domain of their operation (i.e., time, phase, or frequency) [16]-[19]. The displacement of the backscattered signals is measured using time delay estimators with respect to the transducer. These measured displacement between sequences of echo signals is basically appeared as a time-shift or phase-shift [14]. In this paper, time-shift estimator is used to find the tissue displacement. Time-shift estimators are vastly used in estimating the tissue motion. The time-shift estimator typically consists of the identification of the maximum/minimum of a pattern matching functions. In ultrasound imaging the performance of many signal processing applications mainly depends on the performance of their time-delay estimators.

In time-delay estimation there are basically two types of techniques are used. These techniques are individual sample tracking and the window-based estimation technique. This thesis is based on estimation of time-delay in ultrasound echo signals using individual sample tracking rather than using the conventional window-based delay estimation technique.

In window-based technique the signal pattern is set according to the shape of the signal within a certain window in the reference echo signal. After that, a matching algorithm is used to find the best match in the delayed echo signal. The complexity and accuracy of these pattern-matching technique plays a huge deal to the performance of the imaging, so, many researchers are employed tradeoffs between complexity and accuracy [16], [20], [21]. Because of the finite sampling intervals factors such as bias and variance are emerged and to reduce these factors interpolation methods such as curve fitting and polynomial interpolation techniques has been introduced [20]. These curve fitting and polynomial interpolation techniques include parabolic fitting [57], spline fitting [49], cosine fitting [59], and grid slope [60].

In window-based technique the delay estimator estimates the average time shift/phase shift of several samples within a specific window. The size of the window and the overlap between windows play a major role on the performance of this time delay estimators. When different window sizes are used [17], [61], [62] then there needs a tradeoff between the signal-to-noise ratio and resolution of the time-shift estimators. The matter gets worse when the time delay estimation uses multiple window sizes.

In this paper, we present a new time-delay estimator based on the tracking of individual samples using a continuous representation of the echo signal. In this paper, we propose a new delay estimation algorithm called the sample tracking algorithm. The sample tracking algorithm is based on 2-D cross correlation technique. Sample tracking provides the time delay estimation with much higher density compared with conventional window-based methods. Sample tracking algorithms have higher sensitivity and resolution compared with traditional delay estimators because they provide the displacement of individual samples. Simulation results show that sample tracking algorithms significantly outperform commonly used window-based algorithms in terms of bias and standard deviation [28].

Considering in mind the cost of computation it could be maintain that as in this paper a RF sample tracking method is used which is less computation costly than the RF window-based time delay estimation technique as it is already discussed above. Another thing that can be anticipated

from the flow charts of the both conventional flow chart and proposed flow chart that instead of calculating gradient of delay, extract ROI and interpolation and doing strain imaging, a MATLAB surf tool is used to visualize the correlation between the pre- and post- compression rf data.

So, from the above discussion it can be concluded that the proposed ultrasound imaging method is less computation costly than the conventional ultrasound strain imaging.

6.2 Future Work

This thesis work is based on 2-D model which could not represent pragmatic scenario enough. To make this model more practical this proposed method could applied to a 3-D model [63]. There are number 3-D deformable model such as mass-spring, Laplacian surface and meshless model exists [64]-[67]. So, a 3-D model could be designed for simulation using this proposed method as a further work.

The simulations performed in this thesis are all computer-generated simulation. So, another future work related to this thesis could be the use of a real phantom which could give us a practical scenario of the proposed method for clinical application.

REFERENCES

[1] Timoshenko, S. P. and Goodier, J. N. *Theory of Elasticity*, pp. 403–409 (McGraw-Hill, New York), 1970.

[2] Cheney, M. Inverse boundary-value problems. *Am. Scientist*, 85, pp. 448–455, 1997.

[3] Carton, R. W., Clark, J. W., Barron, A. and Dainauskas, J. Estimation of tissue elasticity of the lung. *J. Appl. Physiol.*,19, pp. 236–242, 1964.

[4] Hayes, W. C. and Mockros, L. F. Viscoelastic properties of human articular cartilage. *J. Appl. Physiol.*, 1971, 31, 562–568.

[5] Krokosky, E. M. and Krouskop, T. A. A stress deformation model of the human aorta. *J. Biomed. Mater. Res.*, 2, pp. 503–525, 1968.

[6] Krokosky, E. M. and Krouskop, T. A. The determination of the constitutive relationships for a human aorta. *J. Biomed. Mater. Res.*, 4, pp. 525–547, 1970.

[7] Md. Maruf Hossain Shuvo, A. B. M. Aowlad Hossain, and Krishna Chandra Roy, "Ultrasound Strain Imaging Based on Information Theoretic Delay Estimation," *17th Int'l Conf. on Computer and Information Technology, Daffodil International University, Dhaka, Bangladesh,* pp. 401-405, 22-23 December 2014.

[8] J. Ophir, I. Cespedes, H. Ponnekanti, Y. Yazdi, and X. Li, "Elastography: A quantitative method for imaging the elasticity of biological tissues," *Ultrason. Imaging*, vol. 13, pp. 111–134, Apr. 1991.

[9] A. Heimdal, A. Stoylen, H. Torp, and T. Skjaerpe, "Real-time strain rate imaging of the left ventricle by ultrasound," *J. Am. Soc. Echocardiogr.*, vol. 11, pp. 1013–1019, Nov. 1998.

[10] L. N. Bohs, B. H. Friemel, and G. E. Trahey, "Experimental velocity profiles and volumetric flow via two-dimensional speckle tracking," *Ultrasound Med. Biol.*, vol. 21, no. 7, pp. 885–898, 1995.

[11] M. Lubinski, S. Emelianov, and M. O'Donnell, "Speckle tracking methods for ultrasonic elasticity imaging using short-time correlation," *IEEE Trans. Ultrason. Ferroelectr. Freq. Control*, vol. 46, pp. 82–96, Jan. 1999.

[12] S. Srinivasan and J. Ophir, "A zero-crossing strain estimator in elastography," *Ultrasound Med. Biol.*, vol. 29, no. 2, pp. 227–238, Feb. 2003.

[13] C. Kasai, K. Namekawa, A. Koyano, and R. Omoto, "Real-time two-dimensional blood flow imaging using an autocorrelation technique," *IEEE Trans. Sonics Ultrason.*, vol. 32, no. 3, pp. 458–464, 1985.

[14] T. Loupas, R. Peterson, and R. Gill, "Experimental evaluation of velocity and power estimation for ultrasound blood flow imaging, by means of a two-dimensional autocorrelation approach," *IEEE Trans. Ultrason. Ferroelectr. Freq. Control*, vol. 42, pp. 689–699, Jul. 1995.

[15] H. Torp, K. Kristoffersen, and B. Angelsen, "Autocorrelation techniques in color flow imaging. Signal model and statistical properties of the autocorrelation estimates," *IEEE Trans. Ultrason. Ferroelectr. Freq. Control*, vol. 41, no. 5, pp. 604–612, Sep. 1994.

[16] F. Viola and W. Walker, "A comparison of the performance of time-delay estimators in medical ultrasound," *IEEE Trans. Ultrason. Ferroelectr. Freq. Control*, vol. 50, pp. 392–401, Apr. 2003.

[17] G. Pinton, J. Dahl, and G. Trahey, "Rapid tracking of small displacements with ultrasound," *IEEE Trans. Ultrason. Ferroelectr. Freq. Control*, vol. 53, pp. 1103–1117, June 2006.

[18] I. Hein and W. O'Brien, "Current time-domain methods for assessing tissue motion by analysis from reflected ultrasound echoes—A review," *IEEE Trans. Ultrason. Ferroelectr. Freq. Control*, vol. 40, pp. 84–102, Mar. 1993.

[19] G. Pinton and G. Trahey, "Continuous delay estimation with polynomial splines," *IEEE Trans. Ultrason. Ferroelectr. Freq. Control*, vol. 53, pp. 2026–2035, Nov. 2006.

[20] G. Jacovitti and G. Scarano, "Discrete time techniques for time delay estimation," *IEEE Trans. Acoust. Speech Signal Process.*, vol. 41, pp. 525–533, Feb. 1993.

[21] S. Langeland, J. Dapos, H. Torp, B. Bijnens, and P. Suetens, "A simulation study on the performance of different estimators for twodimensional velocity estimation," in *Proc. IEEE Ultrasonics Symp.*, vol. 2, pp. 1859–1862, Oct. 8–11, 2002.

[22] M. B. Hisham, Shahrul Nizam Yaakob, Raof R. A. A, A. B A. Nazren, N.M.Wafi, "Template Matching Using Sum of Squared Difference and Normalized Cross Correlation", *IEEE Student Conference on Research and Development (SCOReD)*,pp 100-104, 2015.

[23] Hiroaki Niitsuma, Tsutomu Maruyama, "Sum of Absolute Difference Implementations for image processing on FPGAs*", 2010 International Conference on Field Programmable Logic and Applications*, pp 167-170.

[24] Anton1 Fertner and Anders Sjolund, "Comparison of Various Time Delay Estimation Methods by Computer Simulation", IEEE Transactions on Acoustics, Speech, and Signal Processing, Vol. ASSP-34, no. *5,* October 1986, pp 1329-1330.

[25] https://en.wikipedia.org/wiki/Cross-correlation.

[26] T. Varghese, J. Ophir, E. Konofagou, F. Kallel, and R. Righetti, "Tradeoffs in elastographic imaging, ultrasonic imaging," *Ultrason. Imaging*, vol. 23, pp. 216–248, Oct. 2001.

[27] H. Shi and T. Varghese, "Two-dimensional multi-level strain estimation for discontinuous tissue," *Phys. Med. Biol.*, vol. 52, pp. 389–401, Nov. 2007.

[28] C. Sumi, "Fine elasticity imaging utilizing the iterative RF-echo phase matching method," *IEEE Trans. Ultrason. Ferroelectr. Freq. Control*, vol. 46, pp. 158–166, Jan. 1999.

[29] Reza Zahiri-Azar, Septimiu E. Salcudean, "Time-Delay Estimation in Ultrasound Echo Signals Using Individual Sample Tracking*", IEEE Transactions on Ultrasonics, Ferroelectrics, and Frequency Control*, vol. 55, no. 12, pp 2640-2650, December 2008.

[30] Mohammad Arafat Hussain, Emran Mohammad Abu Anas, S. Kaisar Alam, Soo Yeol Lee, and Md. Kamrul Hasan, "Direct and Gradient-Based Average Strain Estimation by Using Weighted Nearest Neighbor Cross-Correlation Peaks", *IEEE Transactions on Ultrasonics, Ferroelectrics, and Frequency Control*, vol. 59, no. 8, pp 1713-1728, August 2012.

[31] J. Ophir, I. Cespedes, B. S. Garra, H. Ponnekanti, Y. Huanga, and N. Maklad, "Elastography: Ultrasonic imaging of tissue strain and elastic modulus in vivo," *Eur. J. Ultrasound*, vol. 3, no. 1, pp. 49–70,1996.

[32] E. I. Céspedes, J. Ophir, H. Ponnekanti, and N. Maklad, "Elastography: Elasticity imaging using ultrasound with application to muscle and breast in vivo," *Ultrason. Imaging*, vol. 15, no. 2, pp. 73–88, 1993.

[33] J. Ophir, S. K. Alam, B. S. Garra, F. Kallel, E. E. Konofagou, T. Krouskop, C. R. B. Merritt, R. Righetti, R. Souchon, S. Srinivasan, and T. Varghese, "Elastography: Imaging the elastic properties of soft tissues with ultrasound," *J. Med. Ultrasound*, vol. 29, pp.155–171, Winter 2002.

[34] R. Zahiri-Azar and S. E. Salcudean, "Motion estimation in ultrasound images using time domain cross correlation with prior estimates," *IEEE Trans. Biomed. Eng.*, vol. 53, no. 10, pp. 1990–2000, 2006.

[35] S. K. Alam, "Novel spline-based approach for robust strain estimation in elastography," *Ultrason. Imaging*, vol. 32, no. 2, pp. 91–102, 2010.

[36] S. K. Alam, J. Ophir, and E. E. Konofagou, "An adaptive strainestimator for elastography," *IEEE Trans. Ultrason. Ferroelectr. Freq. Control*, vol. 45, no. 2, pp. 461–472, 1998.

[37] J. Ophir, S. K. Alam, B. S. Garra, F. Kallel, E. E. Konofagou, T. Krouskop, and T. Varghese, "Elastography: Ultrasonic estimation and imaging of the elastic properties of tissues,'' in *Proc. of the Institute of Mechanical Engineers, Part H: J. Eng. Medicine,* vol. 213, no. 3, pp. 203–233, 1999.

[38] T. Varghese, E. E. Konofagou, J. Ophir, S. K. Alam, and M. Bilgen, "Direct strain estimation in elastography using spectral cross-correlation," *Ultrasound Med. Biol.*, vol. 26, no. 9, pp. 1525–1537, 2000.

[39] S. K. Alam, F. L. Lizzi, T. Varghese, E. J. Feleppa, and S. Ramachandran, "Adaptive spectral strain estimators for elastography," *Ultrason. Imaging*, vol. 26, no. 3, pp. 131–149, 2004.

[40] Gérard Blanchet and Maurice Charbit, "Digital Signal and Image Processing Using MATLAB", 2nd edition, *Wiley-ISTE*, May 22, 2006.

[41] R. C. Gonzalez (Author), R. E. Woods, and S. L. Eddins, "Digital Image Processing Using MATLAB", 3rd Edition, *Gatesmark*, January 1, 2020.

[42] Ultrasonic Transducers Technical Notes, (2011), olympus-ims, pp. 41-48. https://www.olympus-ims.com/en/resources/white-papers/ultrasonic-transducer-technicalnotes/

[43] Carol Rumack and Deborah Levine, "Diagnostic Ultrasound", 5th Edition, *Elsevier*, August 8, 2017.

[44] D. Kane, W. Grassi, R. Sturrock, and P. V. Balint, "A brief history of musculoskeletal ultrasound: From bats and ships to babies and hips", *Rheumatology*, Volume 43, Issue 7, July 1, 2004.

[45] Micheal L Oelze, "Chapter 5-The Acoustic Wave Equation and Simple Solutions", University of Illinois Urbana-Champaign.

[46] E. Okuno, "Chapter-12 Diagnostic Radiology Physics: A Handbook for Teachers and Student", Sao Paulo University.

[47] C. Fung, Biomechanics: Mechanical Properties of Living Tissues, 2nd ed. *Springer-Verlag, New York*, 1993.

[48] Goksel, R. Zahiri-Azar, and S.E. Salcudean, "Simulation of ultrasound radio-frequency signals in deformed tissue for validation of 2d motion estimation with sub-sample accuracy," *Proceedings of the IEEE Eng. Med.Biol. Soc.*, 2007.

[49] Dimitris Manolakis and John G Proakis, *"Digital Signal Processing: Principles, Algorithms, and Applications"* 4th Edition,Prentice Hall, October 5, 1995,pp.116-120.

[50] Buck, John R., Michael M. Daniel, and Andrew C. Singer. *"Computer Explorations in Signals and Systems Using MATLAB"*, 2nd Edition. Upper Saddle River, *NJ: Prentice Hall*, 2002.

[51] Mary Kathryn Thompson, John M. Thompson, "ANSYS Mechanical APDL for Finite Element Analysis", *Elsevier Inc.*, pp 1-6, 2017.

[52] Jørgen Arendt Jensen, "Users' guide for the Field II program", *Technical University of Denmark, Release 3.24*, May 12, 2014.

[53] S. McAleavey, "Field II Tutorial", *University of Rochester Medical Center*, October 27, 2014.

[54] J.A. Jensen, "Field: A Program for Simulating Ultrasound Systems",*10th Nordic-Baltic Conference on Biomedical Imaging Published in Medical & Biological Engineering & Computing*, pp. 351-353, Volume 34, Supplement 1, Part 1, 1996.

[55] K. R. Nightingale, M. L. Palmeri, R. W. Nightingale, and G. E. Trahey, "On the feasibility of remote palpation using acoustic radiation force," *J. Acoust. Soc. Am.*, vol. 110, pp. 625–634, July 2001.

[56] W. F. Walker, F. J. Fernandez, and L. A. Negron, "A method of imaging viscoelastic parameters with acoustic radiation force," *Phys. Med. Biol.*, vol. 45, no. 6, pp. 1437–1447, June 2000.

[57] S. Foster, P. Embree, and W. O'Brien, "Flow velocity profile via time-domain correlation: Error analysis and computer simulation," *IEEE Trans. Ultrason. Ferroelectr. Freq. Control*, vol. 37, pp. 164– 175, May 1990.

[58] B. Geiman, L. Bohs, M. Anderson, S. Breit, and G. Trahey, "A comparison of algorithms for tracking sub-pixel speckle motion." in *Proc. IEEE Ultrasonics Symp*., Oct. 5–8, vol. 2, pp. 1239–1242, 1997.

[59] P. G. de Jong, T. Arts, A. P. Hoks, and R. S. Reneman, "Determination of tissue motion velocity by correlation interpolation of pulsed ultrasonic echo signals," *Ultrason. Imaging*, vol. 12, no. 2, pp. 84–98, Apr. 1990.

[60] B. J. Geiman, L. N. Bohs, M. E. Anderson, S. M. Breit, and G. E. Trahey, "A novel interpolation strategy for estimating subsample speckle motion," *Phys. Med. Biol.*, vol. 45, no. 6, pp. 1541–1552, Jun. 2000.

[61] S. Srinivasan, R. Righetti, and J. Ophir, "Tradeoffs between the axial resolution and the signal-to-noise ratio in elastography," *Ultrasound Med. Biol.*, vol. 29, no. 6, pp. 847–866, Jun. 2003.

[62] F. Walker and E. Trahey, "A fundamental limit on delay estimation using partially correlated speckle signals," *IEEE Trans. Ultrason. Ferroelectr. Freq. Control*, vol. 42, no. 2, pp. 301–308, Mar. 1995.

[63] Zhennan Yan, Shaoting Zhang, S. Kaisar Alam, Dimitris N. Metaxas, Brian S. Garra, Ernest J. Feleppa, "Modulus Reconstruction from Prostate Ultrasound Images using Finite Element Modeling", *Medical Imaging 2012: Ultrasonic Imaging, Tomography, and Therapy,* Proc. of SPIE Vol. 8320, 832016, 2012.

[64] Zhang, S., Gu, L., Huang, P., and Xu, J., "Real-Time Simulation of Deformable Soft Tissue Based on Mass-Spring and Medial Representation," in *Computer Vision for Biomedical Image Applications*, 419–426 ,2005.

[65] Zhang, S., Wang, X., Metaxas, D. N., Chen, T., and Axel, L., "LV Surface Reconstruction from Sparse tMRI using Laplacian Surface Deformation and Optimization," in *International Symposium on Biomedical Imaging*, 698–701, 2009.

[66] Zhang, S., Huang, J., and Metaxas, D. N., "Robust mesh editing using Laplacian coordinates," *Graphical Models* 73, 10–19, 2011.

[67] Wang, X., Chen, T., Zhang, S., Metaxas, D. N., and Axel, L., "LV Motion and Strain Computation from tMRI Based on Meshless Deformable Models," in *Medical Image Computing and Computer Assisted Intervention*, 636–644, 2008.

[68] Sen Zhong, Wei Xia, and Zishu He, "Approximate maximum likelihood time differences estimation in the presence of frequency and phase consistence errors," in *IEEE International Symposium on Signal Processing and Information Technology*, 305-308, 12-15 Dec., 2013.